Drug Delivery and Translational Research
https://doi.org/10.1007/s13346-024-01535-8

ORIGINAL ARTICLE

Impact of calcitriol and PGD_2-G-loaded lipid nanocapsules on oligodendrocyte progenitor cell differentiation and remyelination

Ariane Mwema[1,2] · Viridiane Gratpain[1] · Bernard Ucakar[1] · Kevin Vanvarenberg[1] · Océane Perdaens[3] · Vincent van Pesch[3] · Giulio G. Muccioli[2] · Anne des Rieux[1]

Accepted: 26 January 2024
© Controlled Release Society 2024

Abstract

Multiple sclerosis (MS) is a demyelinating and inflammatory disease of the central nervous system (CNS) in need of a curative treatment. MS research has recently focused on the development of pro-remyelinating treatments and neuroprotective therapies. Here, we aimed at favoring remyelination and reducing neuro-inflammation in a cuprizone mouse model of brain demyelination using nanomedicines. We have selected lipid nanocapsules (LNC) coated with the cell-penetrating peptide transactivator of translation (TAT), loaded with either a pro-remyelinating compound, calcitriol (Cal-LNC TAT), or an anti-inflammatory bioactive lipid, prostaglandin D_2-glycerol ester (PGD_2-G) (PGD_2-G-LNC TAT). Following the characterization of these formulations, we showed that Cal-LNC TAT in combination with PGD_2-G-LNC TAT increased the mRNA expression of oligodendrocyte differentiation markers both in the CG-4 cell line and in primary mixed glial cell (MGC) cultures. However, while the combination of Cal-LNC TAT and PGD_2-G-LNC TAT showed promising results in vitro, no significant impact, in terms of remyelination, astrogliosis, and microgliosis, was observed in vivo in the *corpus callosum* of cuprizone-treated mice following intranasal administration. Thus, although calcitriol's beneficial effects have been abundantly described in the literature in the context of MS, here, we show that the different doses of calcitriol tested had a negative impact on the mice well-being and showed no beneficial effect in the cuprizone model in terms of remyelination and neuro-inflammation, alone and when combined with PGD_2-G-LNC TAT.

Keywords Intranasal · Demyelination · Neuro-inflammation · Nanoparticles · Nose-to-brain

Introduction

Multiple sclerosis (MS) is an autoimmune disease of the central nervous system (CNS) with demyelination, neuroinflammation, and neuroaxonal damage as main pathological hallmarks [1, 2]. This disease affects around 2.8 million people worldwide and is twice as frequent in women than in men. Although treatment options are available, to date, no curative treatment has reached the market yet [3].

It has been well established that vitamin D deficiency is one of the main environmental risk factors of MS. Moreover, it has been associated with MS activity and progression [4]. In addition to its well-known role in calcium homeostasis, several investigations have demonstrated the beneficial effects of vitamin D in the scope of MS, mainly through its active metabolite, calcitriol [5, 6]. Calcitriol has been shown to promote neural stem cell and oligodendrocyte progenitor cells (OPC) differentiation in vitro [7–10], to increase the

Giulio G. Muccioli and Anne des Rieux contributed equally to the work.

✉ Giulio G. Muccioli
giulio.muccioli@uclouvain.be

✉ Anne des Rieux
anne.desrieux@uclouvain.be

[1] Advanced Drug Delivery and Biomaterials, Louvain Drug Research Institute, Université catholique de Louvain, UCLouvain, Avenue E. Mounier 73, 1200 Brussels, Belgium

[2] Bioanalysis and Pharmacology of Bioactive Lipids, Louvain Drug Research Institute, Université catholique de Louvain, UCLouvain, Avenue E. Mounier 73, 1200 Brussels, Belgium

[3] Cellular and Molecular Division, Institute of Neuroscience, Université catholique de Louvain, UCLouvain, Avenue E. Mounier 53, 1200 Brussels, Belgium

Published online: 16 February 2024

expression of growth factors (e.g., nerve growth factor in oligodendrocytes [7, 10] and brain-derived neurotrophic factor (BDNF) in neural stem cells [9]), and therefore potentially to sustain cell survival in the CNS. The mechanism of action of calcitriol involves binding to the intracellular vitamin D receptor (VDR)/retinoic X receptor (RXR) heterodimeric complex [11]. Upon translocation to the nucleus, the calcitriol/VDR/RXR complex binds to specific DNA sequences, the vitamin D responsive elements (VDREs), and modulates the expression of target genes implicated in several pathways including calcium homeostasis, cell differentiation, immunity, and inflammation [6, 12]. This receptor is expressed by several cells of the CNS, including microglia, astrocytes, oligodendrocytes, and activated B and T cells, thus explaining its immunomodulatory effects [6, 13]. Despite its beneficial effects on astrogliosis, microgliosis, and remyelination observed in animal models of MS [14–18], calcitriol has been associated with toxicity and adverse effects (mainly hypercalcemia) [12, 19–22]. To address these limitations and as calcitriol is poorly soluble in physiological fluids, we decided to encapsulate calcitriol in a nanocarrier, namely lipid nanocapsules (LNC) [23, 24]. LNC are suitable for the encapsulation of lipophilic drugs and their components are FDA approved for administration in humans [24–27]. Moreover, the surface of LNC can be modified to increase LNC transport across membranes and/or to the brain (e.g., with cell-penetrating-peptides) or to target specific cells (e.g., oligodendrocyte progenitor cells (OPC)) [24–28]. To further limit systemic adverse effects and promote local delivery to the CNS, we opted for an intranasal administration of calcitriol-loaded LNC (Cal-LNC), with a cell-penetrating peptide (CPP), TAT, at its surface.

Neuro-inflammation is a physio-pathological hallmark of MS and considerably hinders CNS repair. Thus, we hypothesized that by targeting inflammation, in addition to stimulate OPC differentiation, we would support remyelination. We have previously put forth interesting anti-inflammatory properties of prostaglandin D_2-glycerol ester (PGD_2-G), a bioactive lipid, in several in vitro and in vivo models [24, 29–31]. When encapsulated in LNC, we showed that PGD_2-G-LNC was able to decrease the mRNA expression of pro-inflammatory cytokines in the brain of LPS-induced mice following intranasal administration [24]. Moreover, LNC themselves reduced the mRNA levels of pro-inflammatory cytokines and chemokines in experimental autoimmune encephalomyelitis (EAE)-induced mouse brain and spinal cord [24]. However, while TAT-coated PGD_2-G-LNC (PGD_2-G-LNC TAT) decreased neuro-inflammation, they had no significant impact on the mouse clinical score and remyelination process. We therefore combined Cal-LNC TAT with PGD_2-G-LNC TAT with the aim to target both the demyelinating and neuro-inflammatory components of MS.

The efficacy of these formulations was investigated in the cuprizone (CPZ) mouse model, a toxin-based model of demyelination during which consumption of CPZ causes demyelination of specific brain regions, mainly the *corpus callosum*, owing to oligodendrocyte cell death [32]. This process is accompanied by the activation of microglia and astrocytes, followed by spontaneous remyelination upon CPZ withdrawal [32, 33]. The CPZ model was selected as (1) it triggers a highly reproducible form of demyelination in the brain, (2) CPZ is easy to administrate in mouse chow, and (3) it enables a straightforward study of direct remyelinating properties of our formulations [32, 34, 35]. Moreover, numerous studies have provided convincing evidence of the usefulness of this model to assess the efficiency of new therapeutic options aiming at promoting remyelination [36].

Thus, the main goal of this work was to improve CPZ-exposed mice by targeting both the demyelination and neuro-inflammation processes. We have successfully produced and characterized Cal-LNC TAT and tested their efficiency in vitro when used in combination with PGD_2-G-LNC TAT. After assessing the potential toxicity of Cal-LNC TAT, the therapeutic efficacy of Cal-LNC TAT combined with PGD_2-G-LNC TAT was evaluated in the CPZ mouse model following intranasal administration.

Materials and methods

Materials and animals

TAT was purchased from GeneCust (Boynes, France). Dulbecco's modified Eagle medium (DMEM), Trizol, Penicillin-Streptomycin (P/S), and HEPES were purchased from Thermo Fisher Scientific® (Bleiswijk, The Netherlands). Calcitriol was purchased from Win-Win chemical CO., Limited (China). Labrafac® WL1345 was purchased from Gattefossé SA (Saint-Priest, France), Lipoid® S75 from Lipoid Gmbh (Ludwigshafen, Germany), and sodium chloride (NaCl) from Prolabo (Fontenay-sous-bois, France). Kollifor (Solutol) HS15®, Triton™ X-100, sodium pyruvate, insulin, apo-transferrin, biotin, selenium, fetal bovine serum (FBS), charcoal, poly-D-lysine, Amicon® Ultra-0.5 ml 100 K filters, and Dapi were purchased from Sigma Aldrich (Merck, Darmstadt, Germany). Optimal cutting temperature (O.C.T.) compound was purchased from Tissue-Tek, Sakura Finetek (USA). Chloroform, isopropanol, and ethanol were purchased from VWR. Go Script™ Reverse Transcription System and Go Taq qPCR master mix were purchased from Promega® Benelux BV (Leiden, The Netherlands). Prostaglandin D_2 glycerol ester (PGD_2-G) was purchased from Sanbio (Uden, The Netherlands) and Tris-EDTA (TE) buffer from Qiagen®. Normal goat serum was purchased from Labconsult (Ghent). Cuprizone (CPZ, 0.2%)

and control chow were purchased from SSNIFF (Germany). Primers for RT-qPCR were purchased from Integrated D.N.A. technologies (Leuven, Belgium).

In vivo experiments were performed following the Belgian national regulation guidelines in accordance with EU Directive 2010/63/EU and were approved by the ethical committee for animal care of the Université catholique de Louvain medicine faculty (2018/UCL/MD/024) unless stated otherwise. Animals were housed in filter-top cages under artificial light (12-h dark/12-h light) and controlled conditions of temperature (20–22 °C) and had free access to food and drinking water.

Preparation of lipid nanocapsules (LNC)

LNC and calcitriol-loaded LNC (Cal-LNC)

LNC were prepared using the phase inversion temperature method [23, 26, 28, 37]. Briefly, Solutol HS 15 (0.282 g), Lipoïd® S100 (0.025 g), NaCl (0.029 g), Labrafac® WL 1349 (400 µl), and milliQ water (0.9 ml) were mixed under magnetic stirring for 5 min at 40 °C. Three successive temperature cycles were carried out from 60 to 90 °C under constant magnetic stirring. During the last cooling cycle, different amounts of calcitriol or DMSO (vehicle) were added to reach final concentrations ranging from 12 nM to 1 mM in Cal-LNC stock suspension. Ultrapure cold water was then added. The formulations were then filtered using a 0.22-µm filter and stored at 4 °C.

LNC and PGD_2-G-loaded LNC (PGD_2-G-LNC)

LNC were prepared using the phase inversion temperature method with minor adjustments as previously published [24]. In brief, following the homogenization of all the components at 40 °C, 85 µl of the mixture was transferred to an Eppendorf. Three successive temperature cycles were carried out from 60 to 90 °C under constant magnetic stirring. During the last cooling cycle, PGD_2-G or DMSO (vehicle) was added to the mixture to reach a final concentration of 2.34 mM in PGD_2-G-LNC stock suspension. Ultrapure cold water (215 µl) was then added. PGD_2-G-LNC (2.34 mM of PGD_2-G) and blank LNC (LNC) stock solution were filtered using a 0.22-µm filter and stored at 4 °C.

Cell-penetrating peptide (TAT)-coated LNC

TAT-coated LNC were produced by incubating overnight 135 µl of TAT (1 mM in water) with 365 µl of stock-LNC under gentle stirring. LNC without peptide (negative control) were produced by incubating 135 µl of water overnight with 365 µl of stock solution [24, 26].

Characterization of PGD_2-G-LNC and Cal-LNC

Size, polydispersity index (PdI), and zeta-potential (ZP) of LNC were measured using a Malvern Zetasizer Nano ZS (Malvern Instruments). For all measurements, samples were diluted 1/100 (v/v) in water as previously published [24].

The encapsulation efficiency of calcitriol and PGD_2-G was calculated using the formula hereunder:

$$\text{Encapsulation efficiency} = \left(\frac{\text{total amount of compound} - \text{non encapsulated compound}}{\text{compound added in the formulation}} \times 100\right)$$

Calcitriol and PGD_2-G were extracted from LNC by dissolution in methanol at a ratio of 1/20 (*total amount of compound*), as LNC disintegrate in methanol at the aforementioned ratio. Non-encapsulated calcitriol and PGD_2-G were separated from Cal-LNC and PGD_2-G-LNC by ultrafiltration using an Amicon Ultra-0.5 ml 100 K filter. Calcitriol was quantified by high-pressure liquid chromatography (HPLC) coupled to a UV detector (Shimadzu®) using a Machery-Nagel® 125/4 NUCLEODUR 100-5 C 18 column (see Table 1). PGD_2-G was quantified based on a previously described method [24]. Briefly, lipids were extracted and purified in the presence of deuterated standards. The resulting fractions were analyzed by UPLC MS (Xevo TQ-s MS coupled to an Acquity UPLC class H system). Prostaglandin separation was conducted on an Acquity UPLC BEH C18 (150 × 2.1 mm; 1.7 µm) column (Waters) maintained at 40 °C. Mobile phases consisted of H_2O-ACN-acetic acid and ACN-acetic acid used in gradient mode. The mass spectrometer was operated in positive mode (electrospray) and multiple reaction monitoring (MRM) was used to detect the analytes. The MRM transitions determined were as follows: 332.2-> 65.9 (Q) and 332.2-> 315.0 (q) for d4-SEA (used as internal standard); 391.3-> 299.3 (Q) and 391.3-> 373.2 (q) for PGD_2-G. The MassLynx software was used for data acquisition and processing. For each sample, the ratio between

Table 1 Parameters for calcitriol HPLC method

HPLC method	
Mobile phase	Acetonitrile/water (70/30, v/v)
Flow rate	1 ml/min (isocratic system)
Detector wavelength	269 nm
Injection volume	10 µl

PGD_2-G signal and the internal standard signal was used to normalize data. Calibration curves were performed in the same conditions.

Impact of Cal-LNC TAT and PGD_2-G-LNC TAT on the differentiation of CG-4 cells in vitro

CG-4 cells, a spontaneous immortalized rat OPC cell line, were cultured in a proliferation medium (DMEM, 1% P/S, apo-transferrin (50 µg/ml), biotin (9.8 ng/ml), selenium (40 ng/ml), insulin, B104-conditioned media (30%)) and were seeded at 25,000 cells/well in 6-well plates in a recovery medium (DMEM, 1% P/S, insulin, sodium pyruvate, HEPES). The medium was replaced by a fresh proliferation medium after 30 min. The cells were then cultured overnight under standard conditions at 37 °C in a humidified 5% CO_2 incubator [38]. Afterwards, the cells were co-incubated with Cal-LNC TAT (50 nM of calcitriol), PGD_2-G-LNC TAT (10 nM of PGD_2-G), and a combination of Cal-LNC TAT + PGD_2-G-LNC TAT called Comb LNC TAT hereafter (50 nM and 10 nM of calcitriol and PGD_2-G, respectively), for 8 h in the proliferation medium, followed by 5 days of culture in fresh proliferation medium. Non-encapsulated calcitriol, PGD_2-G, and calcitriol + PGD_2-G as well as LNC TAT and vehicle were used as controls. Following cell incubation, supernatants were collected and Trizol (500 µl) was added to the cells before storage at − 80 °C for subsequent mRNA expression analysis by RT-qPCR.

Influence of Cal-LNC TAT and PGD_2-G-LNC TAT on the differentiation of oligodendrocyte progenitor cells (OPC) in primary mixed glial cells (MGC)

Sprague-Dawley rat pups (P0–P2) were used to generate cortical mixed glial cell (MGC) cultures reported by Miron et al. [39], with the local ethical committee approval (2018/UCL/MD/030). In brief, the brains were dissected and the olfactory bulbs, cerebellum, and meninges were removed. Then, the brains were digested with 40 µg/ml of papain and dissociated mechanically using a G18 syringe followed by a G23 syringe. DMEM medium (4.5 g/l glucose, L-glutamine, pyruvate, 10% FBS (v/v), 1% P/S (v/v)) was used to suspend the cells that were then filtered through a 40-µm strainer. The FBS used in the MGC culture medium was depleted in steroids and calcitriol by incubation with 2.5% (w/v) of activated charcoal for 18 h at 4 °C followed by filtration on 0.22 µm [8]. Cells were seeded at 1×10^6 cells/well in poly-D-lysine (1 µg/ml) coated 24-well plates for 8 days. MGC cultures were then treated with a combination of Cal-LNC TAT and PGD_2-G-LNC TAT (Comb LNC TAT) and controls (calcitriol, PGD_2-G, calcitriol + PGD_2-G, Cal-LNC TAT, PGD_2-G-LNC TAT, LNC TAT, and vehicle) for 8 h, followed by 5 days of culture in fresh DMEM culture. Afterwards, Trizol (200 µl) was added to the cells before storage at − 80 °C for subsequent mRNA expression analysis by RT-qPCR.

Impact of Cal-LNC TAT and/or PGD_2-G-LNC TAT on demyelination and neuro-inflammation following intranasal administration in a mouse CPZ model

To induce demyelination, C57BL/6J male mice (Janvier) were fed chow with 0.2% of CPZ for 6 weeks [40, 41] (Fig. 1). Control mice received chow without CPZ during the same period. After 6 weeks, mice were fed control chow and formulations were intranasally administered every other day for 1 week (regimen 1) or 2 weeks (regimen 2). Mice were divided into five groups (eight mice/group): no CPZ + vehicle, CPZ + vehicle, CPZ + LNC TAT, CPZ + Cal-LNC TAT, CPZ + Comb LNC TAT (Fig. 1). For regimen 1, CPZ + Cal-LNC TAT mice received 100 ng of calcitriol while CPZ + Comb LNC TAT received 100 ng of calcitriol and 20 µg of PGD_2-G. For regimen 2, CPZ + Cal-LNC TAT mice received 50 ng of calcitriol while CPZ + Comb LNC TAT received 50 ng of calcitriol and 20 µg of PGD_2-G.

Mouse weight and food intake were monitored weekly during the course of the experiment. Mice were euthanized 1 week (regimen 1) or 2 weeks (regimen 2) after the beginning of the treatment. CNS tissues were carefully collected and stored for further analysis.

Immunofluorescence staining and quantification

The mouse brains were fixed in PFA 4% for 48 h, transferred in a 20% and then a 30% sucrose solution for 24 h each, embedded in O.C.T. compound, and stored at − 80 °C. Brain sections were obtained using a Cryostar NX70 Cryostat (Thermo Scientific) at a thickness of 10 µm. Myelin content was assessed using Fluoromyelin staining (FM) and immunofluorescence for myelin basic protein (MBP). Astrocytes and microglia were detected using antibodies against glial fibrillary acidic protein (GFAP) and ionized calcium-binding adapter molecule 1 (Iba-1), respectively. Regarding OPC, immunofluorescence for oligodendrocyte transcription factor 2 (Olig2) was used to detect the oligodendrocyte lineage while galactosylceramidase (GalC) was used to assess OPC early differentiation.

Briefly, cryosections were immersed in 10% NGS, 2% BSA, and 0.2% Triton in PBS containing primary antibodies for 1 h at room temperature (RT). After four washes in 0.1% Tween 20 in PBS, the sections were stained with secondary antibodies and Dapi for 1 h at RT. The sections

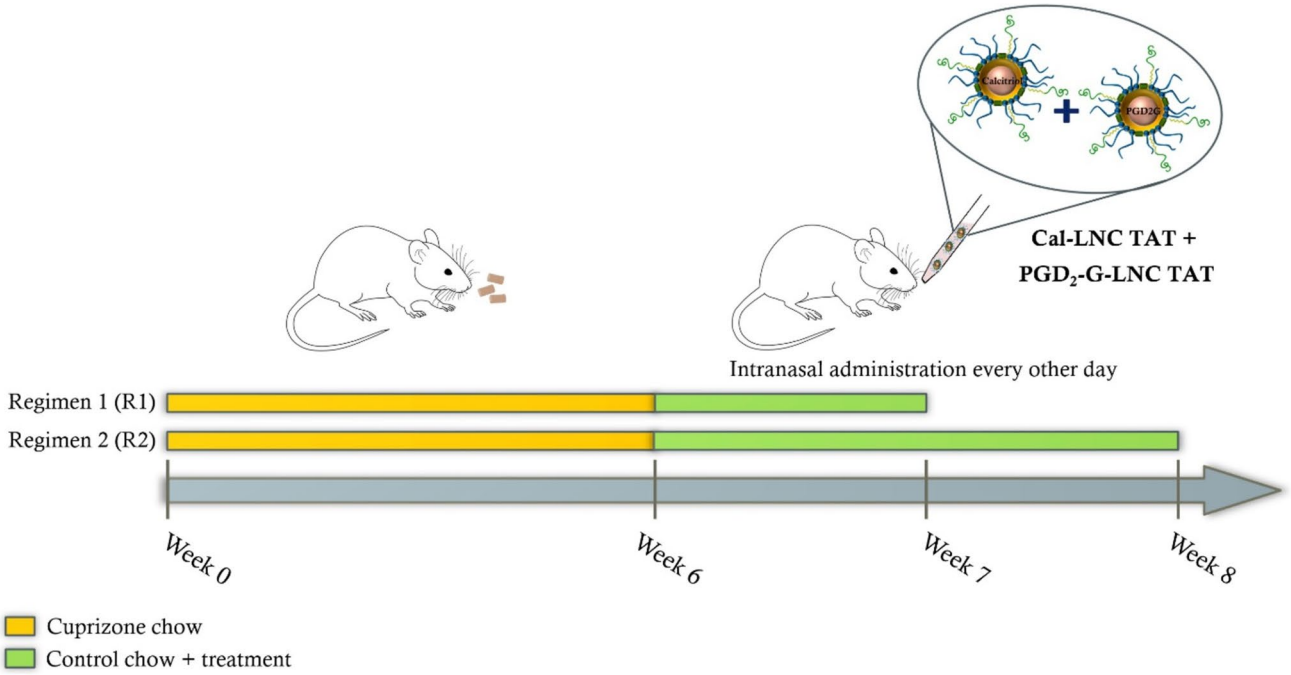


Fig. 1 Timeline of the CPZ studies

were then washed and mounted on slides. Images were acquired using an Axio Scan.Z1 (Zeiss, Germany) slide scanner. Image analysis and quantification were carried out by a researcher, blinded to the group allocation, using AuthorTM version 2023.01 (Visiopharm, Denmark). For the percentage of area occupied by FM, a manual method was applied to identify the area of interest on each slide. Two to three brain slices per animal were analyzed by an experimenter blinded to the treatment allocation and, for each slice, the mean value was calculated in order to obtain a single value per animal. The list of antibodies and stains used is listed in Table 2.

mRNA extraction and real-time qPCR

Total RNA was extracted from cells or tissues using the Trizol reagent (Roche, Basel, Switzerland) according to the manufacturer's instructions. One microgram of total RNA was used to synthesize cDNA with the GoScript Reverse Transcription System. qPCR was performed in duplicate for each sample using the GoTaq SYBR Green mix with a STEP one PLUS instrument and software (Applied Biosystems, Foster City, CA, USA) as previously described [42]. Data are normalized to a reference gene mRNA expression, the 60S ribosomal protein L13 and L19 (RPL13 and RPL19), for rat and murine samples, respectively. We checked that our experimental conditions did not affect the expression of the reference gene for each study. Primer sequences for qPCR are listed in Table 3.

Statistical analysis

Statistical analyses were carried out by one-way ANOVA or two-way ANOVA using Prism 9.00 (GraphPad software, San Diego, CA). Results are expressed as mean ± SEM, unless otherwise stated, and were considered significant if $p < 0.05$. Data deviating from the normal probability (QQ) plot, also known as "outliers," were discarded from the analysis.

Table 2 List of antibodies and stains

Primary antibody	Reference number	Dilution	Secondary antibody	Reference number	Dilution
/	/	/	**Fluoromyelin (FM)**	ThermoFisher, F34651	1/300
Iba-1	Wako, 019–19741	1/1000	DyLight 650	ThermoFisher, SA5-10041	1/500
GFAP-Cy3	Sigma, C9205	1/300	/	/	/
MBP	Abcam, ab7349	1/250	AlexaFluor 647	ThermoFisher, A-21247	1/250
GalC	Millipore, MAB342	1/200	AlexaFluor 594	ThermoFisher, A21155	1/250
Olig2	ThermoFisher, P21954	1/200	AlexaFluor 488	ThermoFisher, A11008	1/250

Table 3 List of primer sequences. Primers for [a]rat and [b]mouse samples

Gene product	Primers 5′-3′		Accession number
	Forward	Reverse	
RPL13[a]	GGCTGAAGCCTACCAGAAAG	CTTTGCCTTTTCCTTCCGTT	NM_173340.2
MBP[a]	CACACACAAGAACTACCCACTAC	GGTGTACGAGGTGTCACAATG	NM_001025291.1 NM_001025292.1 NM_001025293.1 NM_001025294.1 NM_017026.2
MAG[a]	GTGTGTAGCTGAGAACCAGTATG	AGAAGGATTATGGGAGCAAACTC	NM_017190.4
PLP[a]	GGCGACTACAAGACCACCAT	AATGACACACCCGCTCCAAA	NM_030990.3
IL33[a]	CAATCAGGAGACGGTGTGG	GTCCTTGTCATTGGCATTCAG	NM_001014166.1
RPL19[b]	TGACCTGGATGAGAAGGATGAG	CTGTGATACATATGGCGGTCAATC	NM_009078.2 NM_001159483.1
MBP[b]	ACTCACACACGAGAACTACC	GTGTTCGAGGTGTCACAATG	NM_001025251.2 NM_001025254.2 NM_001025255.2 NM_001025256.2 NM_001025258.2 NM_001025259.2 NM_010777.3
iNOS[b]	AGGTACTCAGCGTGCTCCAC	GCACCGAAGATATCTTCATG	NM_010927.4 NM_001313921.1 NM_001313922.1
IL-33[b]	GCCTCCCTGAGTACATACAATG	CGTAGTAGCACCTGGTCTTG	NM_001164724.2 NM_133775.3 NM_001360725.1
IL1-β[b]	TCGCTCAGGGTCACAAGAAA	CATCAGAGGCAAGGAGGAAAAC	NM_008361.4
MIP-1α[b]	AGATTCCACGCCAATTCATC	CTCAAGCCCCTGCTCTACAC	NM_011337.2
Iba-1[b]	CCTGAGGAGATTTCAAAAGCTGA	TGGGACCGTTCTCACACTTC	NM_019467.4

Results

Production and characterization of Cal- and PGD_2-G-loaded LNC TAT

Cal-LNC showed an average size of 60 nm, a PdI lower than 0.2, and a ZP of − 10 mV, regardless of the final concentration of calcitriol in the suspension (Suppl. Table 1). The encapsulation efficiency of calcitriol in LNC ranged from 85 to 100% depending on the initial amount added. Regarding PGD_2-G-LNC, the formulation showed an average size of 60 nm, a PdI lower than 0.2, and a ZP of − 10 mV. The adsorption of TAT at the surface of LNC reduced the ZP by twofolds as previously published [24], regardless of the nature of the cargo (Suppl. Table 1).

Impact of calcitriol and PGD_2-G on the differentiation of CG-4 cells in vitro

Before testing the impact of Cal-LNC TAT and PGD_2-G-LNC TAT on the differentiation of CG-4 cells, optimization of the incubation time and doses of calcitriol and PGD_2-G was carried out.

Calcitriol was thus incubated with CG-4 cells for 8 h or 24 h, and after 5 days of culture, the mRNA expression of several markers of myelinating oligodendrocytes was quantified. Incubation with calcitriol significantly increased the mRNA expression of myelin basic protein (MBP), myelin-associated glycoprotein (MAG), proteolipid protein (PLP), and IL33, a cytokine known to promote OPC differentiation [43, 44], compared to the vehicle after 8 h of treatment (Fig. 2). After 24 h of incubation, calcitriol only significantly increased IL33 mRNA expression.

While the anti-inflammatory effect of PGD_2-G has been well described, its potential effects on myelinating cells have yet to be investigated. In order to study the impact of PGD_2-G, alone or in combination with calcitriol on CG-4 cell differentiation, CG-4 cells were treated with different concentrations of PGD_2-G alone and in combination with calcitriol. Based on the data obtained with calcitriol, cells were treated during 8 h, and the mRNA expression was assessed after 5 additional days in culture. Overall, PGD_2-G alone had no effect on the expression of the markers of interest, apart from IL33 when used at a concentration of 20 nM. When tested in combination with calcitriol, among the different conditions tested, the combination of 50 nM of calcitriol and 10 nM of PGD_2-G

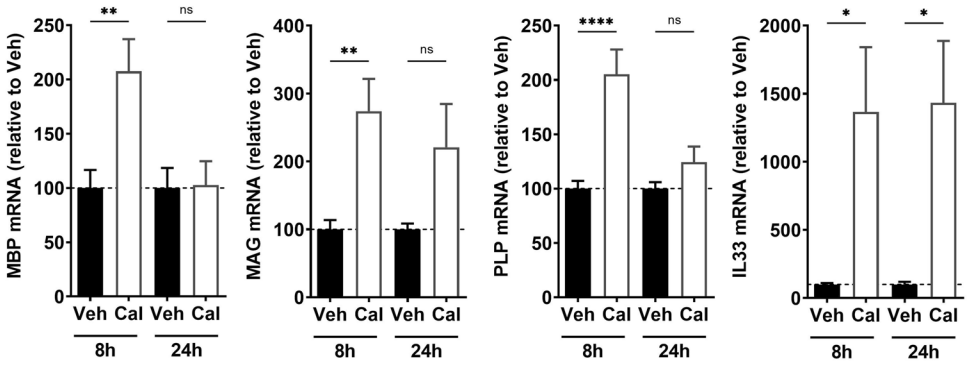


Fig. 2 Impact of calcitriol on CG-4 cell differentiation marker expression. mRNA expression of CG-4 cell differentiation markers was quantified by RT-qPCR after 5 days of culture following 8 h or 24 h of incubation with calcitriol (Cal, 50 nM). The data are reported relative to the expression in vehicle-treated cells (Veh) (both at 8 h and 24 h). Data are expressed as mean ± SEM ($N = 3$, $n = 4$), Sidak's multiple comparisons test, ns—not significant

showed the greatest increase in MBP, MAG, and IL33 mRNA expression compared to the vehicle (Fig. 3). The combination of 20 nM of PGD_2-G with calcitriol showed a similar effect on PLP mRNA expression as the combination with 10 nM of PGD_2-G (Fig. 3).

Impact of Cal-LNC TAT and PGD_2-G-LNC TAT on the differentiation of CG-4 cells in vitro

As shown above, calcitriol and PGD_2-G showed interesting effects on CG-4 cell differentiation. Therefore, as the

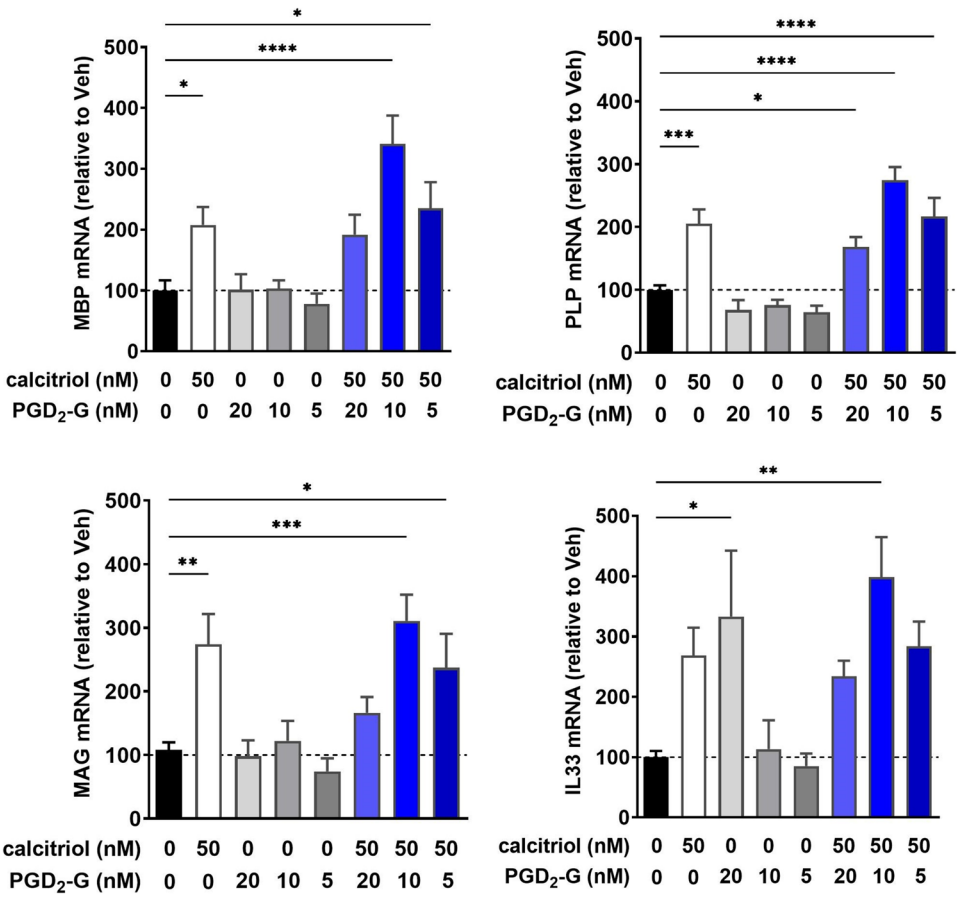


Fig. 3 Impact of the combination of calcitriol and PGD_2-G on CG-4 cells. mRNA expression of CG-4 cell differentiation markers was quantified by RT-qPCR after 5 days of culture following 8 h of incubation with calcitriol (Cal) (50 nM) and different concentrations of PGD_2-G. The incubation of both calcitriol (50 nM) and different concentrations PGD_2-G was also assessed. The data are reported relative to the expression in vehicle-treated cells (Veh). Data are expressed as mean ± SEM ($N = 3$, $n = 3, 4$), Dunnett's multiple comparisons test, $*p < 0.05$, $**p < 0.01$, $***p < 0.001$, $****p < 0.0001$

ultimate goal of the study was to administer a combination of Cal-LNC TAT and PGD_2-G-LNC TAT (Comb LNC TAT in short) intranasally, the next step was to assess whether the encapsulation of the compounds into LNC would not affect their impact on the cells. Incubation of CG-4 cells for 8 h with Comb LNC TAT significantly increased MBP, PLP, MAG, and IL33 mRNA expression compared to vehicle, similar to the coincubation of free calcitriol and PGD_2-G (Comb in short) (Fig. 4). No significant impact was observed when the cells were treated with PGD_2-G, PGD_2-G-LNC TAT, or LNC TAT alone (Fig. 4). However, LNC TAT tended to increase IL33 mRNA expression ($p = 0.1$).

Impact of Cal-LNC TAT and PGD_2-G-LNC TAT on the differentiation of OPC in MGC in vitro

The impact of the combined formulation was also assessed in an MGC culture, composed of microglia, astrocytes, oligodendrocytes, and OPC [39]. Using this culture system has the advantage of assessing the effect on primary OPC in a complex cellular environment thus somewhat closer to

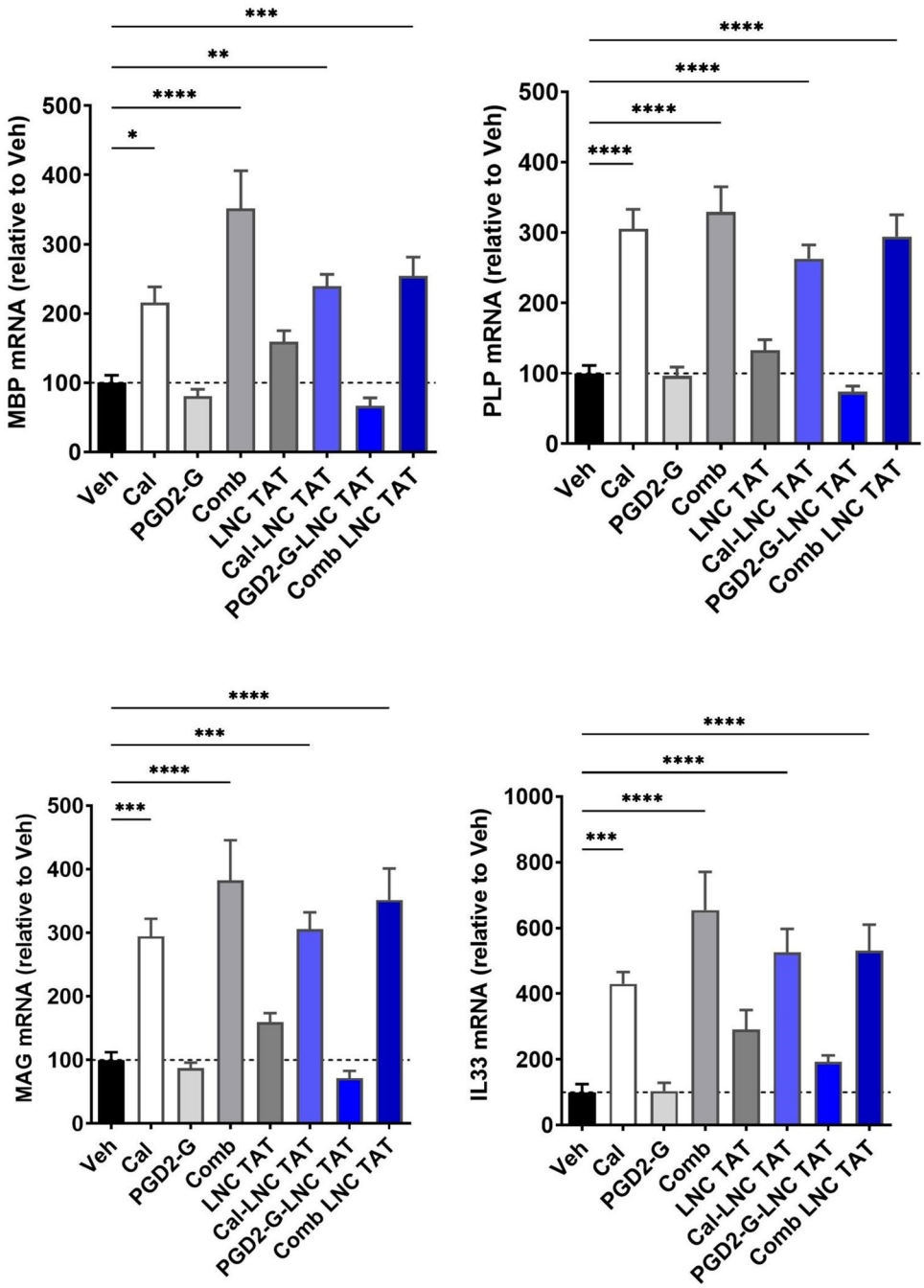


Fig. 4 Impact of Comb LNC TAT on CG-4 cells. mRNA expression of CG-4 cell differentiation markers was quantified after 5 days of culture following 8 h of treatment with Cal-LNC TAT (50 nM of calcitriol) in combination with PGD_2-G-loaded LNC TAT (10 nM of PGD_2-G) (Comb LNC TAT) and controls by RT-qPCR compared to the vehicle (Veh). Data are expressed as mean ± SEM ($N = 3$, $n = 3, 4$), Dunnett's multiple comparisons test, *$p < 0.05$, **$p < 0.01$, ***$p < 0.001$, ****$p < 0.0001$

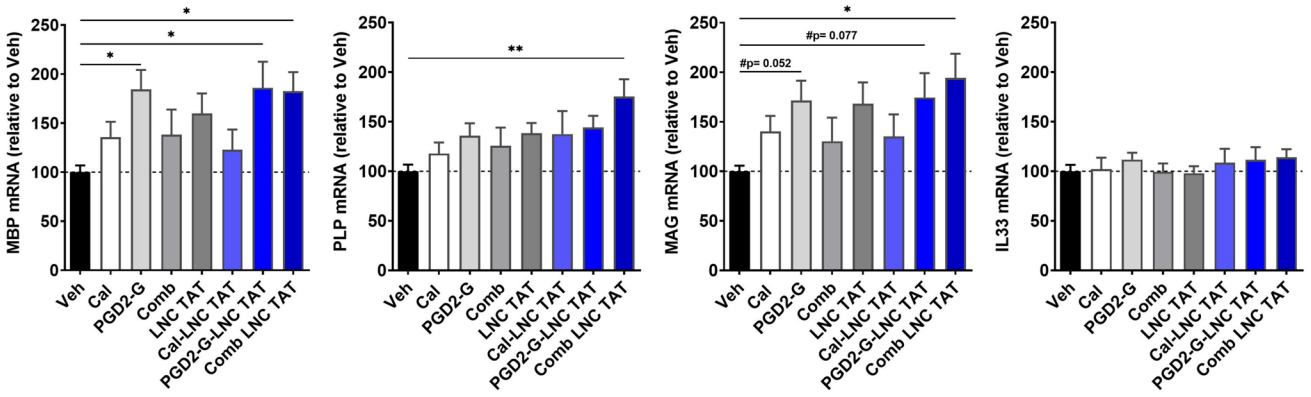


Fig. 5 Impact of Comb LNC TAT on OPC differentiation in an MGC culture. mRNA expression of oligodendrocyte differentiation markers in MGC was quantified after 5 days of culture following 8 h of treatment with Cal-LNC TAT (50 nM of calcitriol) in combination with PGD_2-G-loaded LNC TAT (10 nM of PGD_2-G) (Comb LNC TAT) and controls by RT-qPCR compared to the vehicle (Veh). Data are expressed as mean ± SEM ($N=2$, $n=5$, 6), Dunnett's multiple comparisons test, $*p<0.05$, $**p<0.01$, $***p<0.001$, $****p<0.0001$

the in vivo situation. As for CG-4 cells, the MGC culture was incubated with the different formulations, as well as free drugs, for 8 h. When analyzed 5 days after incubation, Comb LNC TAT increased the mRNA expression of MBP, PLP, and MAG. MBP mRNA expression was also increased compared to vehicle when cells were treated with PGD_2-G, both free and encapsulated (Fig. 5). The latter only showed a trend to increase MAG mRNA expression ($p=0.052$ for PGD_2-G and $p=0.077$ for PGD_2-G-LNC TAT). None of the formulations showed an impact on IL33 mRNA expression (Fig. 5).

Impact of Cal-LNC TAT and PGD_2-G-LNC TAT in cuprizone-induced mice after intranasal administration

Next, the impact of Cal-LNC TAT in combination with PGD_2-G-LNC TAT was evaluated in a CPZ mouse model. Indeed, (1) calcitriol has shown beneficial effects in several models of MS (CPZ and EAE) [14, 17, 18, 45, 46]; (2) previous studies from our lab have shown that PGD_2-G-LNC exert anti-inflammatory properties in the brain following nasal administration [24]; and (3) Cal-LNC TAT in combination with PGD_2-G-LNC TAT increases the expression of OPC differentiation markers in vitro. As the CPZ model can simulate the process of demyelination and remyelination, it serves as a suitable model for myelin regeneration therapies [47].

First, a preliminary study was carried out to optimize the N2B delivery of up to 40 µl of LNC, which is required to administrate the combination of the two formulations (Suppl. data 1). The biodistribution of fluorescent LNC TAT (LNC-DiR TAT) was carried out after intranasal administration of either 20 µl (2 × 5 µl/nostril or 4 × 2.5 µl/nostril with a 3-min pause between administration of both nostrils) or 40 µl (4 × 5 µl/nostril with a similar pause) of the formulation, using an IVIS imaging system. Administration of 40 µl of LNC-DiR TAT significantly increased fluorescent signals in the cranial base (at the cribriform plate region), both 1 and 2 h following nasal administration, and in the brain at 2 h post-administration, compared to the other groups (Suppl. data 1). These preliminary observations encouraged us to use this administration protocol for our studies, despite the observed leakage in the mice's lungs and stomach, as observed by other studies [48–50]. Afterwards, a second study was carried out on healthy mice to evaluate the impact of daily intranasal administration of different doses of Cal-LNC TAT on mice weight. The initial goal was to administer the formulation every day for 2 weeks. However, regardless of the administered dose, mice significantly lost weight after 9 days of administration of Cal-LNC TAT compared to the control mice (LNC TAT) (Suppl. data 2). In light of these observations, treatment with the formulations was discontinued after that period of time.

Based on the range of calcitriol doses used in several mouse models in the literature [14, 16, 17, 51] and the results obtained in our preliminary experiment, mice were treated with Cal-LNC TAT (either 100 ng of calcitriol/mice for 1 week (regimen 1) or 50 ng of calcitriol/mouse for 2 weeks (regimen 2)), following an initial 6-week period of CPZ exposure. The dose of calcitriol was halved in regimen 2 to reduce its potential toxicity while increasing the duration of the treatment compared to regimen 1 to compensate for the smaller dose. Indeed, several bioactive molecules (including anti-inflammatory drugs) have increased remyelination in mice *corpus callosum* when administered after CPZ exposure [52–56]. Treatments with Cal-LNC TAT were administered every other day, alone or in combination with PGD_2-G-LNC TAT (20 µg of PGD_2-G/mouse).

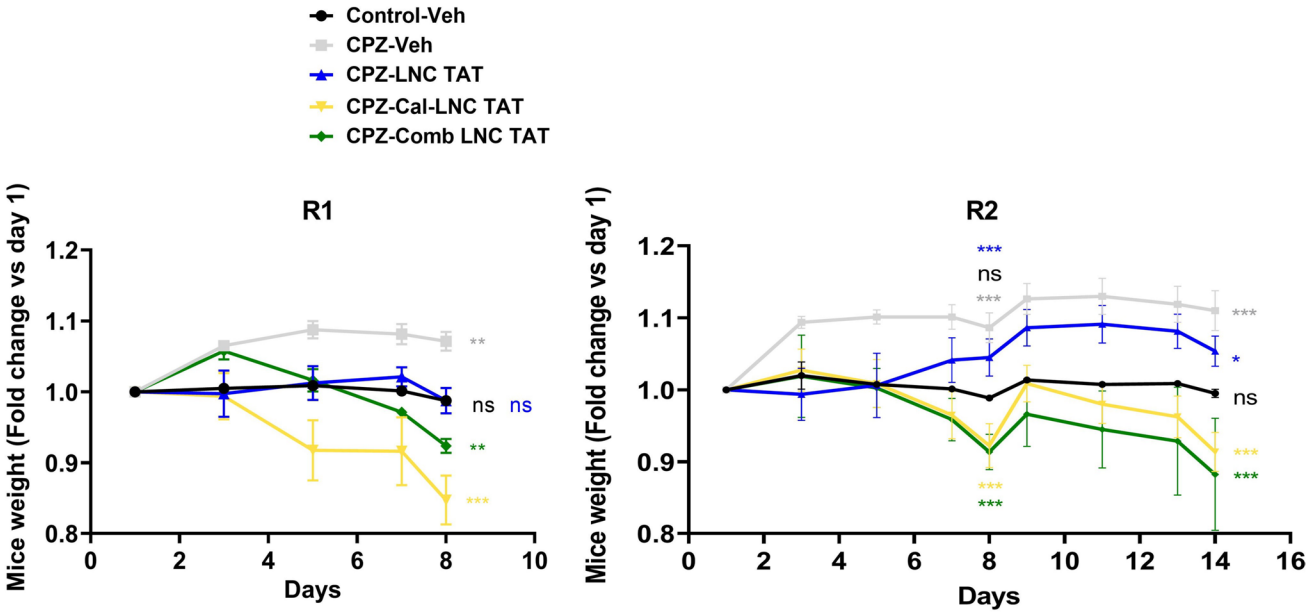


Fig. 6 Impact of Comb LNC TAT on CPZ mouse weight. Mice were fed cuprizone chow for 6 weeks and then received normal chow for 1 (R1) or 2 weeks (R2) together with intranasal administration of the treatment (or vehicle) every other day. For regimen 1 (R1), CPZ mice were treated with either vehicle, LNC TAT, Cal-LNC TAT (100 ng of calcitriol/mouse), or the combination of Cal-LNC TAT (100 ng of calcitriol/mouse) and PGD_2-G-LNC TAT (20 µg of PGD_2-G/mouse) (Comb LNC TAT for short). For regimen 2 (R2), CPZ mice were treated with either vehicle, LNC TAT, Cal-LNC TAT (50 ng of calcitriol/mouse), or the combination of Cal-LNC TAT and PGD_2-G-LNC TAT (Comb LNC TAT, 50 ng of calcitriol and 20 µg of PGD_2-G/mouse). Mice weight was monitored daily starting treatment and is expressed as fold change compared to the mice weight at day 1 of treatment. $n = 8$ per group, 2-way ANOVA, Dunnett's multiple comparisons test compared to mice weight at day 1 of treatment, $^*p < 0.05$, $^{**}p < 0.01$, $^{***}p < 0.001$, ns—not significant

Control mice showed a significant increase in weight during the course of the experiment compared to cuprizone-treated mice (data not shown). During treatment, all calcitriol-treated groups (Cal-LNC TAT and Comb LNC TAT) showed a progressive decrease in weight compared to day 1 of treatment, with a significant difference after 1 week and 2 weeks of treatment (Fig. 6). LNC TAT-treated mice maintained their weight (R1) or increased their weight (R2) during treatment (Fig. 6) and the non-treated mice gained weight following cuprizone withdrawal, for both regimens.

To evaluate the impact of the treatment on myelin, Fluoromyelin stain was quantified in the *corpus callosum* of treated mice. Indeed, in the CPZ mouse model, extensive demyelination, resulting from oligodendrocyte cell death, is mainly observed in the *corpus callosum* of mice [32, 40]. Feeding the mice with 0.2% CPZ significantly decreased Fluoromyelin-stained area, in both regimens (Figs. 7 and 8). These results were confirmed when quantifying by immunofluorescence the MBP-stained area in CPZ-treated mice *corpus callosum* compared to control-fed mice (Suppl. data 3A, B).

No significant impact on Fluoromyelin-stained area was observed for any of the treatments, apart from a trend to increase Fluoromyelin-stained area when mice were treated with LNC TAT for 2 weeks (R2) ($p = 0.07$) (Figs. 7 and 8). Two weeks of treatment with Cal-LNC TAT increased GalC- and Olig2-stained area compared to the vehicle-treated group (Suppl. data 3A, C, D). Olig2 staining was also significantly increased in the Comb LNC TAT group compared to the vehicle-treated group (R2).

The impact of the formulations on microglia and astrocytes was also assessed. For both regimens, CPZ treatment increased GFAP- and iba-1-stained area in the mice *corpus callosum* (Figs. 7 and 8). After 1-week treatment of Cal-LNC TAT, mice showed a significant reduction of iba-1-stained area compared to the non-treated group (CPZ-Veh) (Figs. 7 and 8), the latter was not observed after 2 weeks of treatment. The other formulations had no significant impact on iba-1-stained nor GFAP-stained area for both regimens.

Finally, as the formulations were administered intranasally and as the prefrontal cortex and brainstem are the closest regions of the brain linked to the nasal cavity via the olfactory and trigeminal routes [57, 58], respectively, the impact of the formulation was also assessed on those brain regions (Figs. 9 and 10).

Among the inflammatory markers assessed in the prefrontal cortex, feeding mice with CPZ only induced an increased mRNA expression of MIP-1α, which was not affected by the administration of the formulations (Fig. 9). This was also the case in the brainstem and cerebellum (Fig. 10). In the cortex,

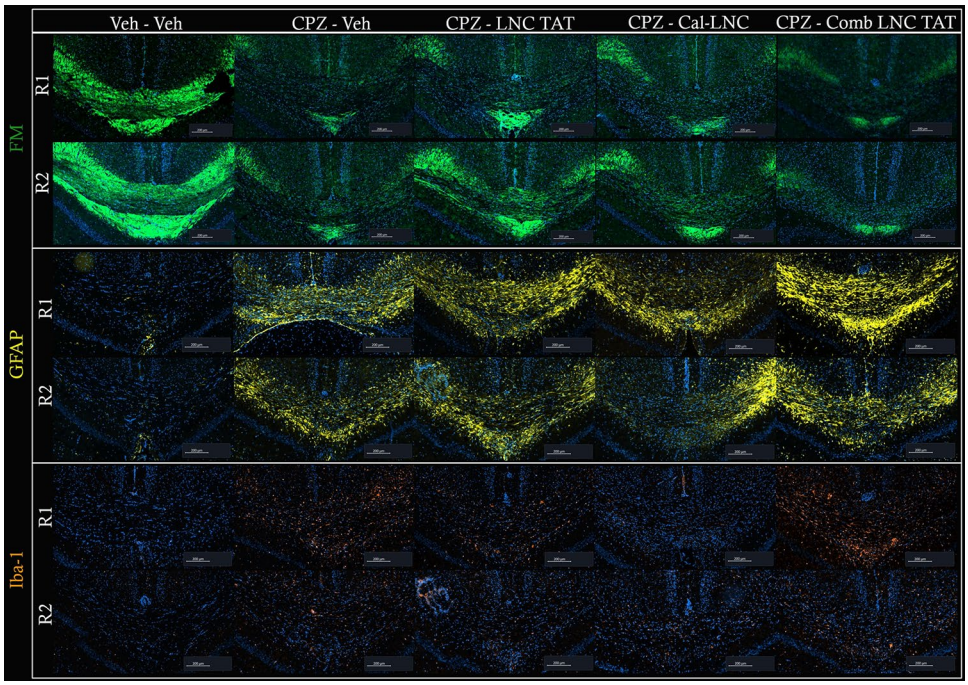


Fig. 7 Impact of Comb LNC TAT on remyelination, astrocyte, and microglia activation in CPZ mouse *corpus callosum*. Mice were fed cuprizone chow for 6 weeks and then received normal chow for 1 (R1) or 2 weeks (R2) together with treatment. The combination of Cal-LNC TAT and PGD_2-G-LNC TAT (Comb LNC TAT (100 ng of calcitriol + 20 µg of PGD_2-G/mouse for R1 and 50 ng of calcitriol + 20 µg of PGD_2-G/mouse for R2)) was administered intranasally every other day. Fluoromyelin (FM), reactive astrocytes (GFAP), and activated microglia (iba-1) were imaged in mice *corpus callosum*

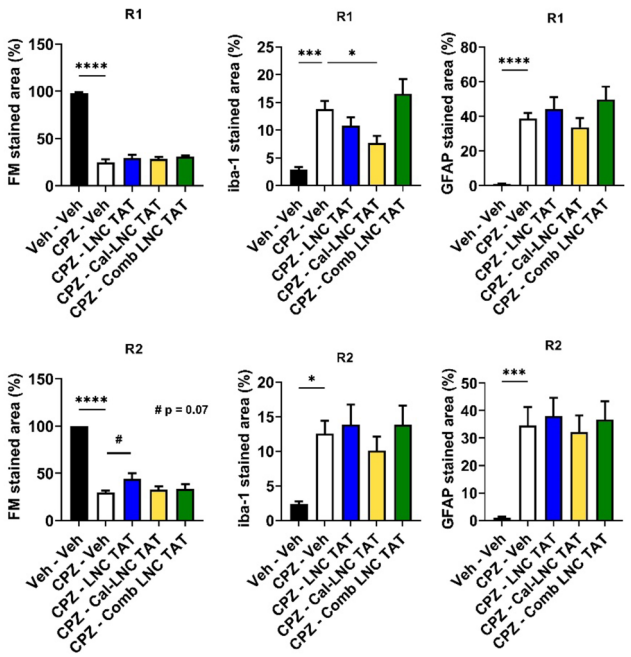


Fig. 8 Impact of Comb LNC TAT on myelin and on astrocyte and microglia activation in CPZ mouse *corpus callosum*. Mice were fed cuprizone chow for 6 weeks and then received normal chow for 1 (R1) or 2 weeks (R2) together with treatment. The combination of Cal-LNC TAT and PGD_2-G-LNC TAT (Comb LNC TAT (100 ng of calcitriol + 20 µg of PGD_2-G/mouse for R1 and 50 ng of calcitriol + 20 µg of PGD_2-G/mouse for R2)) was administered intranasally every other day. Fluoromyelin (FM), reactive astrocytes (GFAP), and activated microglia (iba-1) fluorescent-stained area were quantified in mice *corpus callosum*. $n = 8$ per group, Dunnett's multiple comparisons test compared to CPZ-Veh, $^{*}p < 0.05$, $^{**}p < 0.01$, $^{***}p < 0.001$, $^{****}p < 0.0001$

IL-33 mRNA expression was decreased by CPZ intake, and was further decreased by Cal-LNC TAT administration (regimen 1). In the same setting, iNOS mRNA expression was also decreased (although it was not affected by CPZ intake) in the prefrontal cortex and in the brainstem and cerebellum.

Discussion

Research in the scope of MS has recently focused on increasing remyelination and delivering neuroprotective drugs to patients in addition to therapies targeting inflammation. Several compounds promoting oligodendroglial differentiation and neuroprotection have shown great promise in several preclinical models [59–61]. However, taking the inflammatory environment surrounding MS lesions into account is essential, as it is assumed to play a critical role in the efficiency of pro-remyelinating/pro-regenerative therapies [62]. In a previous study, we targeted neuro-inflammation by intranasal delivery of TAT-coated LNC loaded with a bioactive lipid with anti-inflammatory properties, PGD_2-G (PGD_2-G-LNC TAT) in an EAE mouse model [24]. While an impact on neuro-inflammation was observed, PGD_2-G-LNC TAT did not affect the mice's clinical score and remyelination process. We thus hypothesized that targeting both remyelination and neuro-inflammation using a combination of PGD_2-G-LNC TAT and LNC TAT encapsulating a pro-remyelinating drug would increase the efficacy of our system. We have selected calcitriol for its capacity to promote OPC differentiation and its beneficial immunomodulatory properties in MS models [6]. Calcitriol was encapsulated

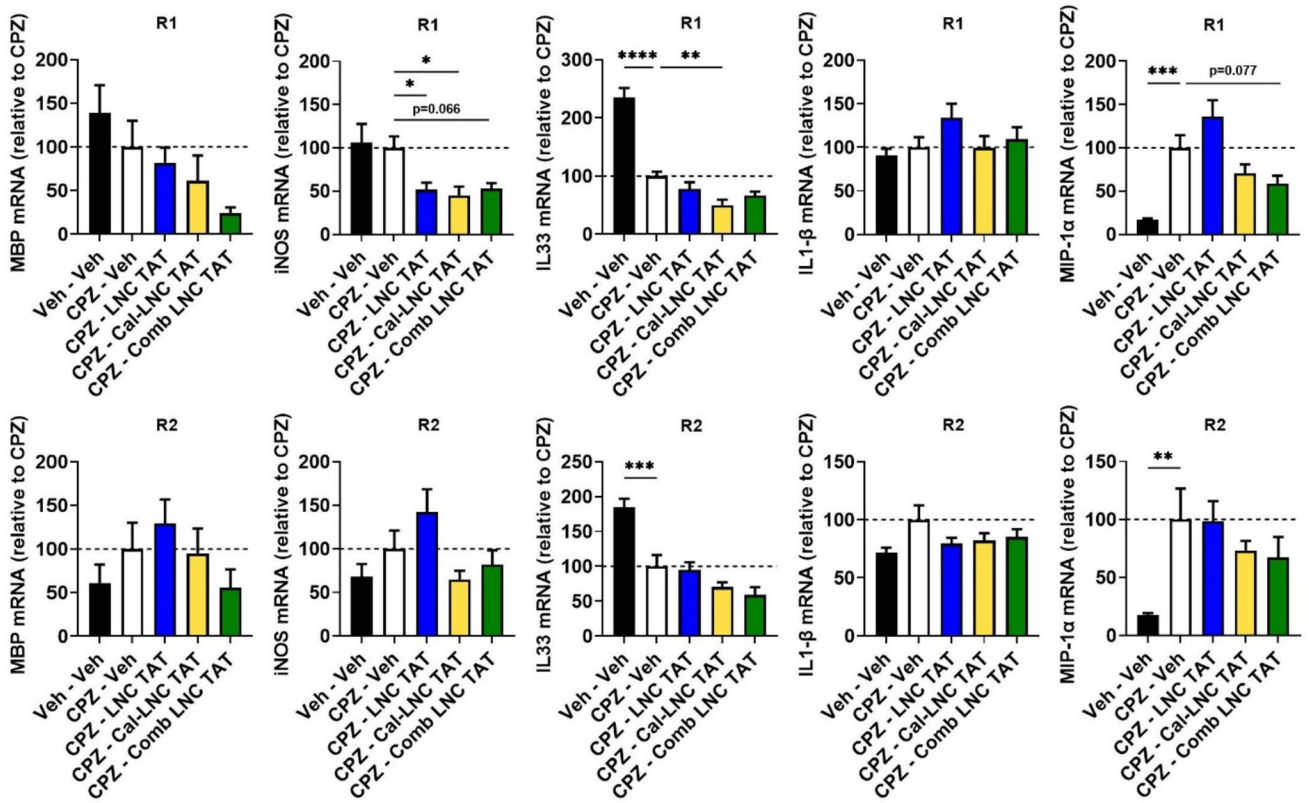


Fig. 9 Impact of Comb LNC TAT on MBP and pro-inflammatory cytokine mRNA expression in CPZ mouse prefrontal cortex. Mice were fed cuprizone chow for 6 weeks and then received normal chow for 1 (R1) or 2 weeks (R2) together with treatment. The combination of Cal-LNC TAT and PGD_2-G-LNC TAT (Comb LNC TAT (100 ng of calcitriol + 20 µg of PGD_2-G/mouse for R1 and 50 ng of calcitriol + 20 µg of PGD_2-G/mouse for R2)) was administered intranasally every other day. mRNA expression of MBP and pro-inflammatory cytokines was quantified in mice prefrontal by RT-qPCR. $n = 8$ per group, Dunnett's multiple comparisons test compared to CPZ-Veh, $^{*}p < 0.05$, $^{**}p < 0.01$, $^{***}p < 0.001$, $^{****}p < 0.0001$

in LNC TAT to improve its solubilization in biological fluids. The resulting formulation was characterized and its efficacy was assessed in vitro and in vivo in combination with PGD_2-G-LNC TAT. While the combined formulations increased OPC differentiation in vitro (i.e., CG-4 cells and MGC cultures), no major impact was observed in CPZ-exposed mice, following intranasal administration.

In line with other studies with lipophilic drugs, we obtained high encapsulation efficiency in LNC for both PGD_2-G and calcitriol [27, 63–65]. Encapsulation of both compounds did not significantly influence LNC characteristics as previously described by our team [24, 27]. To our knowledge, we are the first group to encapsulate PGD_2-G in a nanocarrier [24]; however, nanoparticles such as liposomes, emulsion-templated nanocapsules, and PLGA have been used to deliver calcitriol as therapy for neurodegenerative disorders [66] or to target specific tumor and/or inflammatory cells [67–73]. We have selected LNC as they are more stable, their formulation does not require the use of organic solvents, and they have shown promising results when encapsulating PGD_2-G [24, 25].

The efficacy of the combined formulations to increase OPC differentiation in vitro was first assessed using CG-4 cells [74, 75]. After several trials with different incubation times and PGD_2-G concentrations, we found that the incubation of calcitriol (50 nM) with PGD_2-G (10 nM) for 8 h was the best combination to increase the mRNA expression of key markers of OPC differentiation and IL33, a cytokine reported to promote myelin repair and OPC differentiation [43, 44]. Importantly, these effects were maintained after encapsulation of the compounds in TAT-coated LNC. While the calcitriol effect on OPC differentiation is corroborated by other studies and shown to be mediated via the VDR/RXR pathway [8, 9], we were the first to assess PGD_2-G impact on those cells. PGD_2-G exerts its anti-inflammatory effects via the prostaglandin D2 receptor 1 (DP1) and through the action of its metabolite on the peroxisome proliferator-activated receptor gamma (PPARγ) [30]. CG-4 cells express the DP1 receptor (data not shown); however, no information regarding their capacity to express PPARγ has been reported. Although PGD_2-G (both free and encapsulated) did not induce differentiation of the cells, its

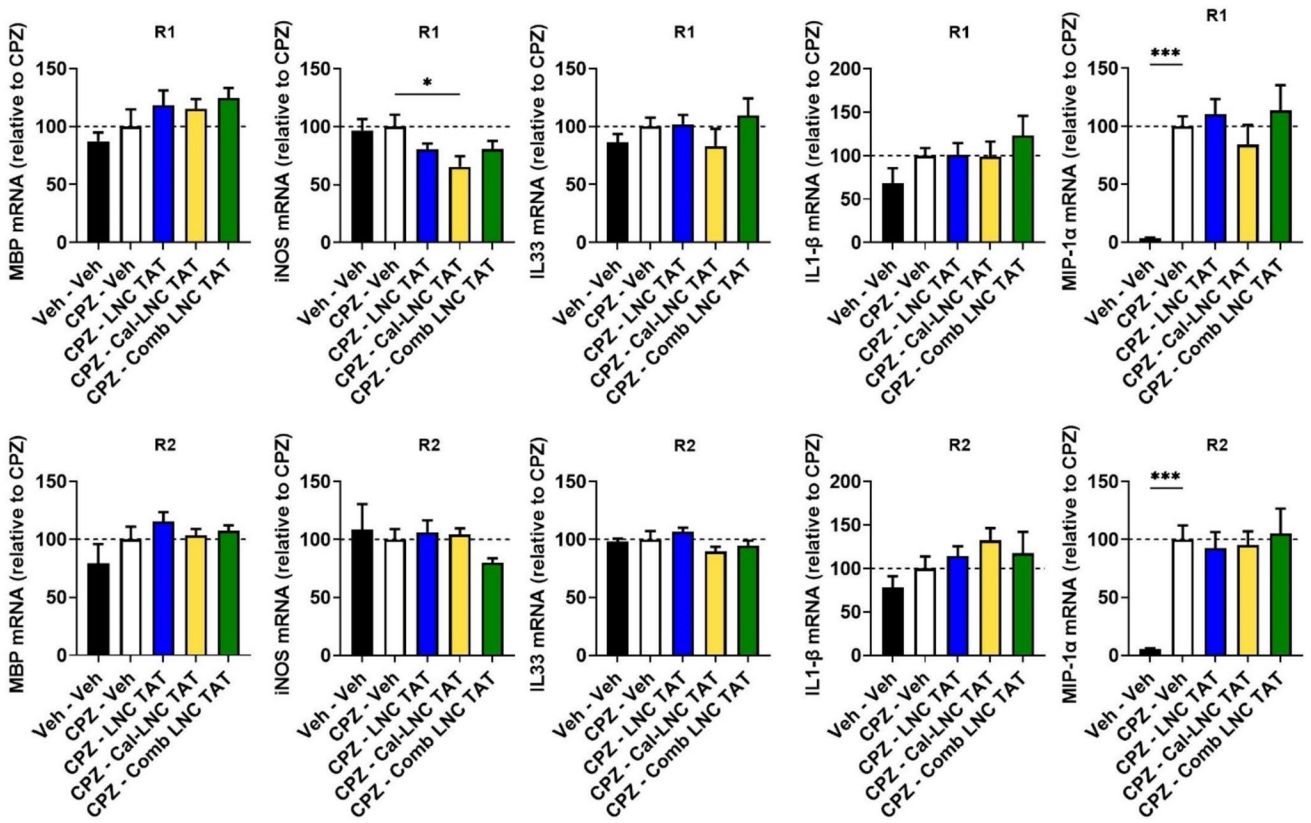


Fig. 10 Impact of Comb LNC TAT on MBP and pro-inflammatory cytokine mRNA expression in CPZ mouse caudal brain. Mice were fed cuprizone chow for 6 weeks and then received normal chow for 1 (R1) or 2 weeks (R2) together with treatment. The combination of Cal-LNC TAT and PGD_2-G-LNC TAT (Comb LNC TAT (100 ng of calcitriol + 20 µg of PGD_2-G/mouse for R1 and 50 ng of calcitriol + 20 µg of PGD_2-G/mouse for R2)) was administered intranasally every other day. mRNA expression of MBP and pro-inflammatory cytokines was quantified in mice hindbrain by RT-qPCR. $n = 8$ per group, Dunnett's multiple comparisons test compared to CPZ-Veh, $^{*}p < 0.05$, $^{**}p < 0.01$, $^{***}p < 0.001$, $^{****}p < 0.0001$

ability to significantly increase IL33 mRNA expression in a concentration-dependent manner could be partly mediated via the DP1 or PPARγ pathway. Indeed, PPARγ agonists have been shown to promote OPC differentiation [76, 77].

In the MGC cultures, Comb LNC TAT was the only condition able to significantly increase MBP, PLP, and MAG mRNA expression, however, to a lesser extent than the effect observed on CG-4 cells (around 1.8 folds vs 3 folds). Moreover, this effect seems to be mainly mediated by PGD_2-G-LNC TAT rather than Cal-LNC TAT, as PGD_2-G-LNC TAT (and PGD_2-G) incubation with MGC significantly increased mRNA expression of MBP and tended to increase expression of MAG. This effect could be explained by the capacity of PGD_2-G (both free and encapsulated) to reduce M1 macrophage/microglia activation [24, 29, 30]. Indeed, it has been shown that the reduction of M1 macrophages promotes oligodendrocyte differentiation [39, 78] and that reducing the inflammatory microenvironment surrounding MS lesions alleviates oligodendrocyte differentiation blockade in MS [62]. The ability of LNC to reduce BV2 cell activation [24] could also explain how LNC induced an increase (albeit not statistically significant) in MBP, MAG, and IL33 mRNA expression. The low impact observed with calcitriol and Cal-LNC TAT as well as the other formulations compared to their impact on CG-4 cells could be due to the action of the other cells in culture (e.g., phagocytosis by macrophages), reducing thus the availability of the treatments to OPC.

The use of high doses of calcitriol in systemic treatments is hindered by the risk of hypercalcemia and hyperphosphatemia, which in turn may lead to renal insufficiency [66, 79]. Several studies have tried to overcome this limitation by encapsulating calcitriol in nanocarriers to promote accumulation at the sites of inflammation [69], in tumor tissue [67, 68, 70, 71], or by targeting specific cell types such as macrophages [72], to eventually reduce the toxic effects caused by systemic uptake. Here, in addition to the encapsulation of calcitriol, we decided to use the intranasal route. Indeed, it enables direct transport to the CNS with reduced peripheral side effects. This approach was shown to potentiate the efficacy in MS mouse models of teriflunomide and IFN-β (compared to conventional administration routes) [80, 81].

Intranasal delivery of free calcitriol has been reported in other studies, in the scope of brain injury prevention (30, 60, and 120 ng/kg) [82] and allergic rhinitis (0.02 µg/mouse daily for 1 week) [83]. We have previously shown that LNC were able to reach the brain following nasal administration and even more so with TAT coated at their surface [24]. However, Mohsen et al. suggested that the systemic pathway, rather than the olfactory pathway, plays a major role in brain delivery following nasal administration of LNC [64], suggesting that a proportion of the intranasally administered dose enters the circulation. We thus conducted a toxicity study on healthy mice by delivering different doses of calcitriol, ranging from 0.1 to 1 µg/mouse (with a similar amount of LNC TAT), via daily intranasal administration of Cal-LNC TAT compared to control (LNC TAT). Regardless of the dose of calcitriol administered, a significant weight loss was observed accompanied by diarrhea. These effects were absent in the LNC TAT-treated mice, suggesting thus that the deleterious effects were due to calcitriol administration. These symptoms were slightly delayed in the group receiving 1 µg of calcitriol every other day, suggesting that reducing the frequency of administration, even at higher doses, delays the toxicity in mice. Alternatively, Azari et al. showed that hydration with saline could also reduce mortality and toxicity in mice receiving calcitriol via intraperitoneal (i.p.) injections [21]. Another option would be to reduce the intranasal administered volumes as much as possible, to maintain the formulation in the nasal cavity [84], and possibly decrease systemic leakage and the subsequent toxicity of calcitriol in our experimental setting. On the other hand, using some of the several developed nasal drug delivery devices that promote deposition of the drugs to the olfactory epithelium (e.g., the Precision Olfactory Delivery® [85] or the Unit Dose system [86]) would allow a greater delivery to the brain with significantly less entry into the circulation. These strategies would only be beneficial if calcitriol toxicity is not CNS-driven. To the best of our knowledge and based on the literature, all the clinical symptoms reported for vitamin D toxicity are manifested from the effects of increased calcium blood levels [87]. To our knowledge, no toxicities have been reported for PGD_2-G nor intranasally administered calcitriol, so we opted to deliver the highest dose of PGD_2-G in accordance with LNC entrapment capacities (20 µg of PGD_2-G) in combination with 100 ng or 50 ng of calcitriol every other day for 1 or 2 weeks, respectively.

We then assessed the efficiency of our formulations in the CPZ mouse model as it is specifically used to analyze non-autoimmune-mediated demyelination and spontaneous remyelination processes combined with therapeutic effects [88]. CPZ exposure for 5–6 weeks induces oligodendrocyte cell death followed by microglia and astrocyte activation, which will in turn maintain a cytotoxic environment against oligodendrocytes leading to demyelination, followed by recovery after CPZ is removed from the diet [32, 89, 90]. In our study, CPZ exposure leads to a transient weight loss that was recovered after CPZ withdrawal, an effect also observed by several teams [14, 52, 91]. However, other studies have reported no significant impact of CPZ exposure on mice weight [92, 93]. CPZ exposure also leads to a significant decrease in Fluoromyelin and MBP staining, supporting CPZ-induced demyelination, and an increase of iba-1 (microglia marker)- and GFAP (reactive astrocytes maker)-stained area in the *corpus callosum* of CPZ mice compared to control. While no significant impact was observed for any of our formulations in terms of remyelination, 1-week treatment with Cal-LNC TAT reduced iba-1 staining in mice *corpus callosum*, but not after 2 weeks of treatment nor when combined with PGD_2-G-LNC TAT. Cal-LNC TAT also increased GalC- and Olig2-stained area compared to the CPZ-Veh group (in regimen 2) similar to Comb LNC TAT for Olig2.

A possible explanation for the absence of effect on remyelination could be due to the calcitriol mechanism of action. Indeed, the reversible beneficial impact of calcitriol observed in EAE mice has been associated with the immunomodulation of $CD4^+$ T cell and its capacity to hinder the ability of autoreactive T cells to enter the CNS without interfering with their production and activation [94, 95]. As the demyelination process in CPZ mice is a T cell-independent process, this could explain the inconsistent results found in the literature regarding the calcitriol effect in this model. Nystad et al. showed that biweekly treatment of 2 µg of calcitriol/mouse had no negative effects on mice weight and showed a positive effect on remyelination [14]. It was suggested that the calcitriol-induced effects may involve the contribution of calcium-binding proteins (e.g., calretinin) and proteins involved in mitochondrial functions [46]. However, Nystad et al. showed that with the same posology, calcitriol had no influence on axonal regeneration nor remyelination [51]. In our case, more frequent administrations (every other day) of lower doses of Cal-LNC TAT (100 ng and 50 ng/mouse for 1 and 2 weeks, respectively) showed a negative impact on mice weight and no significant impact on remyelination and astrocyte activation in mice *corpus callosum*, even when combined with PGD_2-G-LNC TAT.

The starting point of our treatment could also explain the lack of efficacy. Demonstrating a therapeutic effect of our system in the CPZ model would be clinically more relevant. We thus began the treatment, similar to other studies [53–55], after peak demyelination (after CPZ exposure). However, a 3-week treatment of calcitriol starting during the last week of CPZ exposure significantly increased remyelination and reduced gliosis [14]. A study directly comparing pre-treatment and co-treatment with calcitriol found the former, but not the latter, to protect neurons against

neurotoxicity [96]. Moreover, early intervention with calcitriol has been shown to reduce neuro-inflammation as well as increase remyelination in EAE-induced mice [18]. However, Haghmorad and colleagues showed that calcitriol, administered before and after the onset of clinical symptoms, significantly reduced EAE pathology in mice in a similar manner [16].

Another explanation for the limited effect could be the dose and the frequency of administration. In order to avoid toxicity and to favor the beneficial effects of calcitriol, maybe increasing the administered dose while reducing its frequency of administration could be the best compromise for calcitriol. However, these hypotheses do not explain the lack of efficiency of the combined treatments. Indeed, several studies have shown the efficacy of anti-inflammatory compounds in the CPZ model when given during or after CPZ exposure [52, 54, 91, 92, 97–99]. However, the combination of both formulations (Comb LNC TAT) had no significant impact on remyelination and gliosis in our study. Maybe the mechanisms involved in PGD_2-G-LNC TAT anti-inflammatory properties are not implicated in the CPZ-induced physiopathology. Also, it is possible that the hypercalcemia-induced effects could have hindered/masked PGD_2-G-LNC TAT beneficial effects in calcitriol-treated mice. Indeed, it has been observed that high-dose vitamin D-induced hypercalcemia as well as elevation of calcium serum levels may directly activate T cells, promote their pro-inflammatory function, and aggravate EAE severity in mice [100–102] and that hypercalcemia was associated with the development of severely disabling relapses in MS patients [103]. Although hypercalcemia has been associated with small changes in CSF calcium concentrations [104, 105], the brain is protected from acute changes in calcium plasma concentrations by the low cerebrovascular permeability to calcium [105] and no evidence has reported elevated CNS calcium levels during vitamin D-induced hypercalcemia. Moreover, as we chose a range of concentrations similar to or below those used in the literature [15, 17, 18, 45, 51, 95, 106], it was surprising to see such deleterious effects of calcitriol as they were not reported in the aforementioned studies.

Finally, we have evaluated the expression of pro-inflammatory cytokines as well as MBP in regions of the brain linked to the N2B delivery pathway. Even though most studies focus their analysis in mice *corpus callosum* [18, 91, 97, 98], as it is the most affected region following CPZ exposure, our data suggest that both the prefrontal cortex and caudal regions of the brain were not affected by CPZ treatment in terms of neuro-inflammation, as CPZ exposure did not significantly increase the mRNA expression of pro-inflammatory cytokines compared to the control group. This contradicts studies showing an activation of microglia and astrocytes in the cerebral cortex of CPZ-induced mice [52, 90]. However, we did observe an increase of MIP-1α mRNA expression in the prefrontal cortex of CPZ mice, in line with other studies [107, 108]. However, our data also show an increased expression in the brainstem and cerebellum of CPZ mice. One-week treatment of Comb LNC TAT only reduced the mRNA expression of iNOS and MIP-1α in the prefrontal cortex. These modest effects of Comb LNC TAT only occurred in regimen 1, supporting the hypothesis that calcitriol toxicity in mice (more severe in regimen 2) might have masked the formulations' beneficial effects when administered for 2 weeks.

Overall, the data put forth the deleterious effects of calcitriol when delivered within a nanocarrier via the nasal route. Even though the combined effect of Cal-LNC TAT and PGD_2-G-LNC TAT showed promising results in vitro, these were not translated in vivo in our experimental setting. Nevertheless, this study proposes the potential of a combined therapy targeting both inflammation and demyelination as an interesting therapeutic approach for the treatment of MS. Our system could be used with other pro-remyelinating drugs, such as anacardic acid [109], a phenolic lipid derived from cashew nut shells. Indeed, anacardic acid has been shown to promote OPC differentiation in vitro and its pro-remyelinating properties were highlighted in two MS-relevant in vivo models (CPZ and EAE), with no reported toxicities [110]. However, it is pivotal to assess the potential synergistic effects with PGD_2-G in vitro prior to evaluating the effects of the combination in vivo. As both molecules are lipophilic, encapsulation in LNC TAT to increase their bioavailability and enable their protection against enzymatic proprieties remains an option.

Supplementary Information The online version contains supplementary material available at https://doi.org/10.1007/s13346-024-01535-8.

Acknowledgements We thank Yang J. for the supply of the mixed glial cultures, as well as Paquot A. for the quantification of PGD_2-G. We also thank Dr. Bouzin C. for her excellent support and assistance.

Author contribution Ariane Mwema: conceptualization, validation, formal analysis, investigation, writing—original draft, writing—review and editing, visualization. Viridiane Gratpain: investigation. Océane Perdaens: investigation. Bernard Ucakar: investigation. Kevin Vanvarenberg: investigation. Vincent Van Pesch: writing—review and editing. Giulio G. Muccioli: conceptualization, supervision, validation, writing—review and editing, project administration, funding acquisition. Anne des Rieux: conceptualization, supervision, validation, writing—review and editing, project administration, funding acquisition.

Funding Ariane Mwema was supported by a FRIA doctoral grant funded by FNRS (Belgium). Anne des Rieux is a FNRS Senior Research Associate. This work was supported by grants from the French Community of Belgium (Actions de Recherche, ARC Grant), the Fondation Charcot Stichting, and the UCLouvain ("COVID mandate" and "Patrimoine" Grants).

Data availability The datasets generated during and/or analyzed during the current study are available from the corresponding author on reasonable request.

Declarations

Ethics approval and consent to participate All the animal experiments reported in this paper were performed following the Belgian national regulation guidelines in accordance with EU Directive 2010/63/EU and were approved by the ethical committee for animal care of the Université catholique de Louvain medicine faculty (2018/UCL/MD/024) unless stated otherwise. No human studies have been performed in this study.

Consent for publication Not applicable.

Competing interests The authors declare no competing interests.

References

1. Dendrou CA, Fugger L, Friese MA. Immunopathology of multiple sclerosis. Nat Rev Immunol. 2015;15(9):545–58. https://doi.org/10.1038/nri3871.
2. Thompson AJ, et al. Multiple sclerosis. The Lancet. 2018;391(10130):1622–36. https://doi.org/10.1016/s0140-6736(18)30481-1.
3. Walton C, et al. Rising prevalence of multiple sclerosis worldwide: insights from the Atlas of MS, third edition. Mult Scler. 2020;26(14):1816–21. https://doi.org/10.1177/1352458520970841.
4. Fatima M, et al. Therapeutic role of vitamin D in multiple sclerosis: an essentially contested concept. Cureus. 2022;14(6):e26186. https://doi.org/10.7759/cureus.26186.
5. Burton JM, et al. A phase I/II dose-escalation trial of vitamin D3 and calcium in multiple sclerosis. Neurology. 2010;74(23):1852–9. https://doi.org/10.1212/WNL.0b013e3181e1cec2.
6. Galoppin M, et al. Full spectrum of vitamin D immunomodulation in multiple sclerosis: mechanisms and therapeutic implications. Brain Commun. 2022;4(4):fcac171. https://doi.org/10.1093/braincomms/fcac171.
7. Baas D, et al. Rat oligodendrocytes express the vitamin D(3) receptor and respond to 1,25-dihydroxyvitamin D(3). Glia. 2000;31(1):59–68. https://doi.org/10.1002/(sici)1098-1136(200007)31:1%3c59::aid-glia60%3e3.0.co;2-y.
8. de la Fuente AG, et al. Vitamin D receptor-retinoid X receptor heterodimer signaling regulates oligodendrocyte progenitor cell differentiation. J Cell Biol. 2015;211(5):975–85. https://doi.org/10.1083/jcb.201505119.
9. Shirazi HA, et al. 1,25-Dihydroxyvitamin D3 enhances neural stem cell proliferation and oligodendrocyte differentiation. Exp Mol Pathol. 2015;98(2):240–5. https://doi.org/10.1016/j.yexmp.2015.02.004.
10. Mengozzi M, et al. Vitamins D3 and D2 have marked but different global effects on gene expression in a rat oligodendrocyte precursor cell line. Mol Med. 2020;26(1):32. https://doi.org/10.1186/s10020-020-00153-7.
11. Miao D, Goltzman D. probing the scope and mechanisms of calcitriol actions using genetically modified mouse models. JBMR Plus. 2021;5(1):e10434. https://doi.org/10.1002/jbm4.10434.
12. Janousek J, et al. Vitamin D: sources, physiological role, biokinetics, deficiency, therapeutic use, toxicity, and overview of analytical methods for detection of vitamin D and its metabolites. Crit Rev Clin Lab Sci. 2022;1–38. https://doi.org/10.1080/10408363.2022.2070595.
13. Smolders J, et al. Expression of vitamin D receptor and metabolizing enzymes in multiple sclerosis-affected brain tissue. J Neuropathol Exp Neurol. 2013;72(2):91–105. https://doi.org/10.1097/NEN.0b013e31827f4fcc.
14. Nystad AE, et al. Effect of high-dose 1.25 dihydroxyvitamin D3 on remyelination in the cuprizone model. APMIS. 2014;122(12):1178–86. https://doi.org/10.1111/apm.12281.
15. Chiuso-Minicucci F, et al. Treatment with vitamin D/mog association suppresses experimental autoimmune encephalomyelitis. PLoS ONE. 2015;10(5):e0125836. https://doi.org/10.1371/journal.pone.0125836.
16. Haghmorad D, et al. Prevention and treatment of experimental autoimmune encephalomyelitis induced mice with 1, 25-dihydroxyvitamin D3. Neurol Res. 2019;41(10):943–57. https://doi.org/10.1080/01616412.2019.1650218.
17. Parastouei K, et al. The effect of calcitriol and all-trans retinoic acid on T-bet, IFN-gamma, GATA3 and IL-4 genes expression in experimental autoimmune encephalomyelitis. APMIS. 2020;128(11):583–92. https://doi.org/10.1111/apm.13073.
18. de Oliveira LRC, et al. Calcitriol prevents neuroinflammation and reduces blood-brain barrier disruption and local macrophage/microglia activation. Front Pharmacol. 2020;11:161. https://doi.org/10.3389/fphar.2020.00161.
19. Crocker JF, et al. The comparative toxicity of vitamin D metabolites in the weanling mouse. Toxicol Appl Pharmacol. 1985;80(1):119–26. https://doi.org/10.1016/0041-008x(85)90106-1.
20. Wingerchuk DM, et al. A pilot study of oral calcitriol (1,25-dihydroxyvitamin D3) for relapsing-remitting multiple sclerosis. J Neurol Neurosurg Psychiatry. 2005;76(9):1294–6. https://doi.org/10.1136/jnnp.2004.056499.
21. Azari AA, et al. Hydration with saline decreases toxicity of mice injected with calcitriol in preclinical studies. J Environ Pathol Toxicol Oncol. 2013;32(3):241–4. https://doi.org/10.1615/jenvironpatholtoxicoloncol.2013007532.
22. Lung BE, Mowery ML, Komatsu DEE. Calcitriol. In: StatPearls [Internet]. Treasure Island (FL): StatPearls Publishing; 2023. PMID: 30252281.
23. Heurtault B, Saulnier P, Pech B, Proust JE, Richard J, Benoit JP. Lipidic nanocapsules: preparation process and use as drug delivery systems. Patent No. WO02688000. 2000.
24. Mwema A, et al. Lipid nanocapsules for the nose-to-brain delivery of the anti-inflammatory bioactive lipid PGD(2)-G. Nanomedicine. 2022;1:102633. https://doi.org/10.1016/j.nano.2022.102633.
25. Huynh NT, et al. Lipid nanocapsules: a new platform for nanomedicine. Int J Pharm. 2009;379(2):201–9. https://doi.org/10.1016/j.ijpharm.2009.04.026.
26. Carradori D, et al. NFL-lipid nanocapsules for brain neural stem cell targeting in vitro and in vivo. J Control Release. 2016;238:253–62. https://doi.org/10.1016/j.jconrel.2016.08.006.
27. Carradori D, et al. Retinoic acid-loaded NFL-lipid nanocapsules promote oligodendrogenesis in focal white matter lesion. Biomaterials. 2020;230:119653. https://doi.org/10.1016/j.biomaterials.2019.119653.
28. Labrak Y, et al. Impact of anti-PDGFRalpha antibody surface functionalization on LNC uptake by oligodendrocyte progenitor cells. Int J Pharm. 2022;618:121623. https://doi.org/10.1016/j.ijpharm.2022.121623.
29. Alhouayek M, et al. Implication of the anti-inflammatory bioactive lipid prostaglandin D2-glycerol ester in the control of macrophage activation and inflammation by ABHD6. Proc Natl Acad Sci U S A. 2013;110(43):17558–63. https://doi.org/10.1073/pnas.1314017110.

30. Alhouayek M, et al. The endogenous bioactive lipid prostaglandin D2-glycerol ester reduces murine colitis via DP1 and PPAR-gamma receptors. FASEB J. 2018;32(9):5000–11. https://doi.org/10.1096/fj.201701205R.
31. Buisseret B, et al. Prostaglandin D2-glycerol ester decreases carrageenan-induced inflammation and hyperalgesia in mice. Biochim Biophys Acta Mol Cell Biol Lipids. 2019;1864(5):609–18. https://doi.org/10.1016/j.bbalip.2019.01.009.
32. Zirngibl M, et al. Oligodendrocyte death and myelin loss in the cuprizone model: an updated overview of the intrinsic and extrinsic causes of cuprizone demyelination. Mol Neurodegener. 2022;17(1):34. https://doi.org/10.1186/s13024-022-00538-8.
33. Burrows DJ, et al. Animal models of multiple sclerosis: From rodents to zebrafish. Mult Scler. 2019;25(3):306–24. https://doi.org/10.1177/1352458518805246.
34. Kipp M, et al. Experimental in vivo and in vitro models of multiple sclerosis: EAE and beyond. Mult Scler Relat Disord. 2012;1(1):15–28. https://doi.org/10.1016/j.msard.2011.09.002.
35. Avsar T, et al. Investigation of neuro-inflammatory parameters in a cuprizone induced mouse model of multiple sclerosis. Turk J Biol. 2021;45(5):644–55. https://doi.org/10.3906/biy-2104-88.
36. Leo H, Kipp M. Remyelination in multiple sclerosis: findings in the cuprizone model. Int J Mol Sci. 2022;23(24). https://doi.org/10.3390/ijms232416093.
37. Lloyd AF, et al. Central nervous system regeneration is driven by microglia necroptosis and repopulation. Nat Neurosci. 2019;22(7):1046–52. https://doi.org/10.1038/s41593-019-0418-z.
38. Lourenco T, et al. Modulation of oligodendrocyte differentiation and maturation by combined biochemical and mechanical cues. Sci Rep. 2016;6:21563. https://doi.org/10.1038/srep21563.
39. Miron VE, et al. M2 microglia and macrophages drive oligodendrocyte differentiation during CNS remyelination. Nat Neurosci. 2013;16(9):1211–8. https://doi.org/10.1038/nn.3469.
40. Morell P, et al. Gene expression in brain during cuprizone-induced demyelination and remyelination. Mol Cell Neurosci. 1998;12(4–5):220–7. https://doi.org/10.1006/mcne.1998.0715.
41. Mu HF, et al. Distinctive functional deficiencies in axonal conduction associated with two forms of cerebral white matter injury. CNS Neurosci Ther. 2019;25(9):1018–29. https://doi.org/10.1111/cns.13155.
42. De Berdt P, et al. Stem cells from human apical papilla decrease neuro-inflammation and stimulate oligodendrocyte progenitor differentiation via activin-A secretion. Cell Mol Life Sci. 2018;75(15):2843–56. https://doi.org/10.1007/s00018-018-2764-5.
43. Natarajan C, Yao SY, Sriram S. TLR3 agonist poly-IC induces IL-33 and promotes myelin repair. PLoS ONE. 2016;11(3):e0152163. https://doi.org/10.1371/journal.pone.0152163.
44. Sung HY, et al. Down-regulation of interleukin-33 expression in oligodendrocyte precursor cells impairs oligodendrocyte lineage progression. J Neurochem. 2019;150(6):691–708. https://doi.org/10.1111/jnc.14788.
45. Parastouei K, et al. The effect of 1, 25(OH)2 D3 (calcitriol) alone and in combination with all-trans retinoic acid on ROR-gammat, IL-17, TGF-beta, and FOXP3 gene expression in experimental autoimmune encephalomyelitis. Nutr Neurosci. 2018;21(3):210–8. https://doi.org/10.1080/1028415X.2016.1263039.
46. Oveland E, et al. 1,25-Dihydroxyvitamin-D3 induces brain proteomic changes in cuprizone mice during remyelination involving calcium proteins. Neurochem Int. 2018;112:267–77. https://doi.org/10.1016/j.neuint.2017.08.008.
47. Zendedel A, Beyer C, Kipp M. Cuprizone-induced demyelination as a tool to study remyelination and axonal protection. J Mol Neurosci. 2013;51(2):567–72. https://doi.org/10.1007/s12031-013-0026-4.
48. Gartziandia O, et al. Chitosan coated nanostructured lipid carriers for brain delivery of proteins by intranasal administration. Colloids Surf B Biointerfaces. 2015;134:304–13. https://doi.org/10.1016/j.colsurfb.2015.06.054.
49. Goncalves J, et al. Nose-to-brain delivery of levetiracetam after intranasal administration to mice. Int J Pharm. 2019;564:329–39. https://doi.org/10.1016/j.ijpharm.2019.04.047.
50. Goncalves J, et al. Pre-clinical assessment of the nose-to-brain delivery of zonisamide after intranasal administration. Pharm Res. 2020;37(4):74. https://doi.org/10.1007/s11095-020-02786-z.
51. Nystad AE, Torkildsen O, Wergeland S. Effects of vitamin D on axonal damage during de- and remyelination in the cuprizone model. J Neuroimmunol. 2018;321:61–5. https://doi.org/10.1016/j.jneuroim.2018.05.016.
52. Jia Y, et al. Cordycepin (3'-deoxyadenosine) promotes remyelination via suppression of neuroinflammation in a cuprizone-induced mouse model of demyelination. Int Immunopharmacol. 2019;75:105777. https://doi.org/10.1016/j.intimp.2019.105777.
53. Zhang Y, et al. A dual effect of ursolic acid to the treatment of multiple sclerosis through both immunomodulation and direct remyelination. Proc Natl Acad Sci USA. 2020;117(16):9082–93. https://doi.org/10.1073/pnas.2000208117.
54. Honarvar F, et al. Ursolic acid enhances myelin repair in adult mice brains and stimulates exhausted oligodendrocyte progenitors to remyelinate. J Mol Neurosci. 2022;72(10):2081–93. https://doi.org/10.1007/s12031-022-02059-x.
55. Liu L, et al. Ginsenoside Rg1 promotes remyelination and functional recovery in demyelinating disease by enhancing oligodendrocyte precursor cells-mediated myelin repair. Phytomedicine. 2022;106:154309. https://doi.org/10.1016/j.phymed.2022.154309.
56. Zhu Y, et al. Stemazole promotes oligodendrocyte precursor cell survival in vitro and remyelination in vivo. Int J Mol Sci. 2022;23(18):10756. https://doi.org/10.3390/ijms231810756.
57. Bourganis V, et al. Recent advances in carrier mediated nose-to-brain delivery of pharmaceutics. Eur J Pharm Biopharm. 2018;128:337–62. https://doi.org/10.1016/j.ejpb.2018.05.009.
58. Chatterjee B, et al. Targeted drug delivery to the brain via intranasal nanoemulsion: available proof of concept and existing challenges. Int J Pharm. 2019;565:258–68. https://doi.org/10.1016/j.ijpharm.2019.05.032.
59. Melchor GS, et al. Remyelination pharmacotherapy investigations highlight diverse mechanisms underlying multiple sclerosis progression. ACS Pharmacol Transl Sci. 2019;2(6):372–86. https://doi.org/10.1021/acsptsci.9b00068.
60. Villoslada P, Steinman L. New targets and therapeutics for neuroprotection, remyelination and repair in multiple sclerosis. Expert Opin Investig Drugs. 2020;29(5):443–59. https://doi.org/10.1080/13543784.2020.1757647.
61. Allanach JR, et al. Current status of neuroprotective and neuroregenerative strategies in multiple sclerosis: a systematic review. Mult Scler. 2022;28(1):29–48. https://doi.org/10.1177/13524585211008760.
62. Starost L, et al. Extrinsic immune cell-derived, but not intrinsic oligodendroglial factors contribute to oligodendroglial differentiation block in multiple sclerosis. Acta Neuropathol. 2020;140(5):715–36. https://doi.org/10.1007/s00401-020-02217-8.
63. Giacomeli R, et al. Neuroprotective effects of curcumin lipid-core nanocapsules in a model Alzheimer's disease induced by beta-amyloid 1–42 peptide in aged female mice. Brain Res. 2019;1721:146325. https://doi.org/10.1016/j.brainres.2019.146325.

64. Mohsen K, et al. Intranasal lipid nanocapsules for systemic delivery of nimodipine into the brain: in vitro optimization and in vivo pharmacokinetic study. Mater Sci Eng C Mater Biol Appl. 2020;116:111236. https://doi.org/10.1016/j.msec.2020.111236.
65. El-Sheridy NA, et al. Itraconazole lipid nanocapsules gel for dermatological applications: in vitro characteristics and treatment of induced cutaneous candidiasis. Colloids Surf B Biointerfaces. 2019;181:623–31. https://doi.org/10.1016/j.colsurfb.2019.05.057.
66. Slusarczyk J, et al. Nanocapsules with polyelectrolyte shell as a platform for 1,25-dihydroxyvitamin D3 neuroprotection: study in organotypic hippocampal slices. Neurotox Res. 2016;30(4):581–92. https://doi.org/10.1007/s12640-016-9652-2.
67. Almouazen E, et al. Nano-encapsulation of vitamin D3 active metabolites for application in chemotherapy: formulation study and in vitro evaluation. Pharm Res. 2013;30(4):1137–46. https://doi.org/10.1007/s11095-012-0949-4.
68. Ramalho MJ, et al. PLGA nanoparticles as a platform for vitamin D-based cancer therapy. Beilstein J Nanotechnol. 2015;6:1306–18. https://doi.org/10.3762/bjnano.6.135.
69. Maradana MR, et al. Immunomodulatory liposomes targeting liver macrophages arrest progression of nonalcoholic steatohepatitis. Metabolism. 2018;78:80–94. https://doi.org/10.1016/j.metabol.2017.09.002.
70. Liu C, et al. Tumor-targeted nanoparticles deliver a vitamin D-based drug payload for the treatment of EGFR tyrosine kinase inhibitor-resistant lung cancer. Mol Pharm. 2018;15(8):3216–26. https://doi.org/10.1021/acs.molpharmaceut.8b00307.
71. Nicolas S, et al. Polymeric nanocapsules as drug carriers for sustained anticancer activity of calcitriol in breast cancer cells. Int J Pharm. 2018;550(1–2):170–9. https://doi.org/10.1016/j.ijpharm.2018.08.022.
72. Rafique A, et al. Targeted lipid nanoparticle delivery of calcitriol to human monocyte-derived macrophages in vitro and in vivo: investigation of the anti-inflammatory effects of calcitriol. Int J Nanomedicine. 2019;14:2829–46. https://doi.org/10.2147/IJN.S192113.
73. Cai C, et al. Adventitial delivery of nanoparticles encapsulated with 1alpha, 25-dihydroxyvitamin D3 attenuates restenosis in a murine angioplasty model. Sci Rep. 2021;11(1):4772. https://doi.org/10.1038/s41598-021-84444-x.
74. Louis JC, et al. CG-4, a new bipotential glial cell line from rat brain, is capable of differentiating in vitro into either mature oligodendrocytes or type-2 astrocytes. J Neurosci Res. 1992;31(1):193–204. https://doi.org/10.1002/jnr.490310125.
75. De Vries GH, Boullerne AI. Glial cell lines: an overview. Neurochem Res. 2010;35(12):1978–2000. https://doi.org/10.1007/s11064-010-0318-9.
76. Bernardo A, et al. Peroxisome proliferator-activated receptor-gamma agonists promote differentiation and antioxidant defenses of oligodendrocyte progenitor cells. J Neuropathol Exp Neurol. 2009;68(7):797–808. https://doi.org/10.1097/NEN.0b013e3181aba2c1.
77. Bernardo A, et al. The nuclear receptor peroxisome proliferator-activated receptor-gamma promotes oligodendrocyte differentiation through mechanisms involving mitochondria and oscillatory Ca2+ waves. Biol Chem. 2013;394(12):1607–14. https://doi.org/10.1515/hsz-2013-0152.
78. Chu F, et al. The roles of macrophages and microglia in multiple sclerosis and experimental autoimmune encephalomyelitis. J Neuroimmunol. 2018;318:1–7. https://doi.org/10.1016/j.jneuroim.2018.02.015.
79. Deeb KK, Trump DL, Johnson CS. Vitamin D signalling pathways in cancer: potential for anticancer therapeutics. Nat Rev Cancer. 2007;7(9):684–700. https://doi.org/10.1038/nrc2196.
80. Gadhave DG, Kokare CR. Nanostructured lipid carriers engineered for intranasal delivery of teriflunomide in multiple sclerosis: optimization and in vivo studies. Drug Dev Ind Pharm. 2019;45(5):839–51. https://doi.org/10.1080/03639045.2019.1576724.
81. Gonzalez LF, et al. Intranasal delivery of interferon-beta-loaded nanoparticles induces control of neuroinflammation in a preclinical model of multiple sclerosis: a promising simple, effective, non-invasive, and low-cost therapy. J Control Release. 2021;331:443–59. https://doi.org/10.1016/j.jconrel.2020.11.019.
82. Enkhjargal B, et al. Intranasal administration of vitamin D attenuates blood-brain barrier disruption through endogenous upregulation of osteopontin and activation of CD44/P-gp glycosylation signaling after subarachnoid hemorrhage in rats. J Cereb Blood Flow Metab. 2017;37(7):2555–66. https://doi.org/10.1177/0271678X16671147.
83. Cho SW, et al. Intranasal treatment with 1, 25-dihydroxyvitamin D3 alleviates allergic rhinitis symptoms in a mouse model. Allergy Asthma Immunol Res. 2019;11(2):267–79. https://doi.org/10.4168/aair.2019.11.2.267.
84. Minne A, et al. The delivery site of a monovalent influenza vaccine within the respiratory tract impacts on the immune response. Immunology. 2007;122(3):316–25. https://doi.org/10.1111/j.1365-2567.2007.02641.x.
85. Hoekman JD, Hite M, Brunelle A, Relethford J, Ho RJY. Nasal drug delivery device. US9550036 B2; 2017.
86. Trevino JT, et al. Non-invasive strategies for nose-to-brain drug delivery. J Clin Trials. 2020;10(7).
87. Asif A, Farooq N. Vitamin D toxicity. In: StatPearls [Internet]. Treasure Island (FL); 2022. PMID: 32491799.
88. Praet J, et al. Cellular and molecular neuropathology of the cuprizone mouse model: clinical relevance for multiple sclerosis. Neurosci Biobehav Rev. 2014;47:485–505. https://doi.org/10.1016/j.neubiorev.2014.10.004.
89. Zhan J, et al. The cuprizone model: dos and do nots. Cells. 2020;9(4). https://doi.org/10.3390/cells9040843.
90. Castillo-Rodriguez MLA, et al. Astroglial and oligodendroglial markers in the cuprizone animal model for de- and remyelination. Histochem Cell Biol. 2022;158(1):15–38. https://doi.org/10.1007/s00418-022-02096-y.
91. Hashimoto M, et al. The flavonoid Baicalein attenuates cuprizone-induced demyelination via suppression of neuroinflammation. Brain Res Bull. 2017;135:47–52. https://doi.org/10.1016/j.brainresbull.2017.09.007.
92. Honarvar F, et al. Myelin protection by ursolic acid in cuprizone-induced demyelination in mice. Iran J Pharm Res. 2019;18(4):1978–88. https://doi.org/10.22037/ijpr.2019.112181.13582.
93. Toomey LM, et al. Cuprizone feed formulation influences the extent of demyelinating disease pathology. Sci Rep. 2021;11(1):22594. https://doi.org/10.1038/s41598-021-01963-3.
94. Grishkan IV, et al. 1,25-Dihydroxyvitamin D3 selectively and reversibly impairs T helper-cell CNS localization. Proc Natl Acad Sci USA. 2013;110(52):21101–6. https://doi.org/10.1073/pnas.1306072110.
95. Moore JR, et al. 1,25-Dihydroxyvitamin D(3) increases the methionine cycle, CD4(+) T cell DNA methylation and Helios(+)Foxp3(+) T regulatory cells to reverse autoimmune neurodegenerative disease. J Neuroimmunol. 2018;324:100–14. https://doi.org/10.1016/j.jneuroim.2018.09.008.
96. Ibi M, et al. Protective effects of 1 alpha,25-(OH)(2)D(3) against the neurotoxicity of glutamate and reactive oxygen species in mesencephalic culture. Neuropharmacology. 2001;40(6):761–71. https://doi.org/10.1016/s0028-3908(01)00009-0.
97. Chami M, et al. Acid sphingomyelinase deficiency enhances myelin repair after acute and chronic demyelination. PLoS ONE. 2017;12(6):e0178622. https://doi.org/10.1371/journal.pone.0178622.
98. Aryanpour R, et al. Progesterone therapy induces an M1 to M2 switch in microglia phenotype and suppresses NLRP3

inflammasome in a cuprizone-induced demyelination mouse model. Int Immunopharmacol. 2017;51:131–9. https://doi.org/10.1016/j.intimp.2017.08.007.
99. Yamamoto S, et al. Ursolic acid treatment suppresses cuprizone-induced demyelination and motor dysfunction via upregulation of IGF-1. J Pharmacol Sci. 2020;144(3):119–22. https://doi.org/10.1016/j.jphs.2020.08.002.
100. Hausler D, et al. High dose vitamin D exacerbates central nervous system autoimmunity by raising T-cell excitatory calcium. Brain. 2019;142(9):2737–55. https://doi.org/10.1093/brain/awz190.
101. Hausler D, Weber MS. Vitamin D supplementation in central nervous system demyelinating disease-enough is enough. Int J Mol Sci. 2019;20(1). https://doi.org/10.3390/ijms20010218.
102. Hausler D, Torke S, Weber MS. High-dose vitamin D-mediated hypercalcemia as a potential risk factor in central nervous system demyelinating disease. Front Immunol. 2020;11:301. https://doi.org/10.3389/fimmu.2020.00301.
103. Fragoso YD, et al. Unfavorable outcomes during treatment of multiple sclerosis with high doses of vitamin D. J Neurol Sci. 2014;346(1–2):341–2. https://doi.org/10.1016/j.jns.2014.08.019.
104. Murphy VA, Quentin RS, Stanley IR. Homeostasis of brain and cerebrospinal fluid calcium concentrations during chronic hypo- and hypercalcemia. J Neurochem. 1986;47(6):1735–41. https://doi.org/10.1111/j.1471-4159.1986.tb13082.x.
105. Tai CY, Quentin RS, Stanley IR. Calcium influxes into brain and cerebrospinal fluid are linearly related to plasma ionized calcium concentration. Brain Res. 1986;385(2):227–36. https://doi.org/10.1016/0006-8993(86)91068-1.
106. Lemire JM, Archer DC. 1,25-dihydroxyvitamin D3 prevents the in vivo induction of murine experimental autoimmune encephalomyelitis. J Clin Invest. 1991;87(3):1103–7. https://doi.org/10.1172/JCI115072.
107. Buschmann JP, et al. Inflammatory response and chemokine expression in the white matter corpus callosum and gray matter cortex region during cuprizone-induced demyelination. J Mol Neurosci. 2012;48(1):66–76. https://doi.org/10.1007/s12031-012-9773-x.
108. Clarner T, et al. CXCL10 triggers early microglial activation in the cuprizone model. J Immunol. 2015;194(7):3400–13. https://doi.org/10.4049/jimmunol.1401459.
109. Ljunggren-Rose A, et al. Anacardic acid induces IL-33 and promotes remyelination in CNS. Proc Natl Acad Sci U S A. 2020;117(35):21527–35. https://doi.org/10.1073/pnas.2006566117.
110. Gao YH, et al. Treatment with anacardic acid modulates dendritic cell activation and alleviates the disease development of autoimmune neuroinflammation in mice. Biochem Biophys Res Commun. 2022;613:34–40. https://doi.org/10.1016/j.bbrc.2022.04.115.

Publisher's Note Springer Nature remains neutral with regard to jurisdictional claims in published maps and institutional affiliations.

Springer Nature or its licensor (e.g. a society or other partner) holds exclusive rights to this article under a publishing agreement with the author(s) or other rightsholder(s); author self-archiving of the accepted manuscript version of this article is solely governed by the terms of such publishing agreement and applicable law.